NAZARBAYEV UNIVERSITY

PHOSPHATASE ACTIVITY OF SULFUR DOPED CARBON DOTS

Adilet Dautov
(B.Sc., Nazarbayev University)

A THESIS SUBMITTED
FOR THE DEGREE OF MASTER OF SCIENCE IN BIOLOGICAL SCIENCES
DEPARTMENT OF BIOLOGY SCHOOL OF SCIENCE AND TECHNOLOGY
NAZARBAYEV UNIVERSITY
2020

DECLARATION

I hereby declare that the thesis is my original work and it has been written by me in its entirety. I have duly acknowledged all the sources of information which have been used in the thesis. This thesis has also not been submitted for any degree in any university previously.

_____Adilet Dautov_____

24 January 2021

ACKNOWLEDGEMENTS

I would like to express my gratitude to the Nazarbayev University for providing me with great MSc program. This project would not be possible to finish without all the university staff that were responsible for getting access to laboratories, ordering reagents and setting up necessary equipment. Firstly, I would like to thank Dr. Haiyan Fan for her guidance throughout the course of the project. She provided our lab with carbon dots, aided in characterization and helped me to set up me thesis project. Secondly, I would like to thank our lab member, Lazzat Nurtay, for helping me with most of the experiments, analysis and generation of SEM images. Thirdly, I would like to thank Dr. Yingqiu Xie for providing with all the necessary equipment. Fourthly, I would like to thank my family members and my groupmates for their support, especially in these hard times.

I am grateful to MSc graduate coordinators Dr. Ferdinand Molnar and Dr. Christian Schoenbach for their constant support and guidance. They were very patient and always encouraged me. Also, I want to thank Dr. Vesselin Paunov for reviewing my thesis and giving valuable feedback. Finally, I would like to thank Dr. Philip Enns and Maya Davletova for making it possible to extend my MSc program.

TABLE OF CONTENTS

Nazarbayev University, School of Science and Technology, Department of Biology
Master´s Degree Program in Biology

Adilet Dautov: Phosphatase activity of sulfur doped carbon dots
Master of Science thesis; 43 pages, 0 appendix(es)
Supervisors: Yingqiu Xie, Department of Biology, Haiyan Fan, Department of Chemistry
24.01.2021

Carbon dots, phosphatase, bacteria, growth inhibition

ABSTRACT

Carbon dots are novel class of carbon nanomaterials which recently have attracted a widespread attention due to their strong fluorescence, low-cost production and easy synthesis methods. They have been used mostly in biosensing, bioimaging and as drug delivery agents. Recently it was found that they can have enzyme mimetic activity and thus can act as nanozymes. Carbon dots exhibit peroxidase activity as well as can act as catalysts in electrocatalysis. In this project, a novel property of carbon dots, phosphatase activity was identified, and the working mechanism was investigated. The nitrogen and sulfur doped carbon dots were synthesized through a hydrothermal reaction using beet as the starting material. Using NBT-BCIP and pNPP as the substrates, the phosphatase of several assays was performed on carbon dots including pH, temperature and inhibition screening. The enzymatic kinetics characteristics were quantitatively analyzed and antimicrobial properties were tested. The as prepared carbon dots showed high reactivity with both substrates and were not affected by various pH and temperature conditions. In addition, carbon dots exhibited strong inhibition against the growth of *E. coli,* and rather mild inhibition against *L. lactis* in a dose dependent manner. Thus, the N and S doped carbon dots are likely achieved the phosphatase through the direct participation in the dephosphorylation steps. The antimicrobial effect exhibited on the *E. coli* bacteria might be based on the phosphatase nature of the carbon dots.

LIST OF TABLES

LIST OF FIGURES AND ILLUSTRATIONS

ABBREVIATIONS

CD	carbon dot
BTSCD	beet-derived sulfur doped carbon dots
BTCD	beet-derived carbon dots
BCIP-NBT	5-Bromo-4-chloro-3-indolyl phosphate-nitro blue tetrazolium
pNPP	para-Nitrophenyl Phosphate
ALP	alkaline phosphatase
DH_2O	distilled water
DDH_2O	double distilled water
OD	optical density
RA	relative activity
V_{max}	maximal velocity
K_m	Michaelis-Menten constant
HR-AFM	High-Resolution Atomic Force Microscopy
FT-IR	Fourier-transform infrared spectroscopy
SEM	scanning electron microscopy
ROS	reactive oxygen species
PL	photoluminescence
P_i	inorganic phosphate

1 INTRODUCTION

Nanoscience deals with materials with the size ranging from 1 to 100 nm. One of these nanomaterials are carbon dots. Recently carbon dots have been attracting a lot of attention due to their relatively cheap production and various properties. One of such properties is the enzyme mimetic activity. Because of the enigmatic nature of carbon dots, this property is not studied in depth and it is only starting to develop. My research is designed to investigate this property and thus contribute to repository of information about carbon dots.

1.1 Carbon Dots

Carbon Dots (CDs) are a part of carbon-based nanomaterials which in recent years have attracted a widespread attention. CDs are monodisperse spherical nanoparticles with a skeleton based up on carbon and a large amount of groups that contain oxygen on the surface. The fluorescence of CDs is achieved by careful adjustment of their size and of surface chemical groups (Lim et al., 2015). CDs are composed of sp^2 carbon, oxygen, and nitrogen elements and other doped heteroatoms (Cao et al., 2007). Their size varies from 1 to 100 nm in diameter (Das et al., 2019). Because of their low cost, abundant source, high quantum yield, and high chemical and photo stability, they are seen as potential candidate in bioimaging, bio-sensing, and other related application in biology (Wang & Qiu, 2016). The schematic representation of CDs can be seen on figure 1.

Figure 1. Schematic representation of carbon dots. Adapted from *Semiconductor and carbon-based fluorescent nanodots: the need for consistency* by A.Cayuela, M.L.Soriano, C.Carrilo-Carrión and M.Valcárcel, 2016, *Chemical Communications*, *52*, 1311-1326

1.1.1 Synthesis

CDs were first discovered during the process of purification of single-walled carbon nanotubes fabricated by arc discharge methods by Scrivens in 2004 (Xu et al., 2004). Since that time, various synthetic methods for CDs have been developed along with various starting materials

(Wang & Qiu, 2016). The synthetic methods are generally classified into two groups: "top-down" and "bottom-up" methods. The top-down approach implies cleavage of larger carbonaceous materials, such as carbon nanotubes, graphite, diamond nanocrystals, and commercial activated carbon (Qiao et al., 2010). Some examples of this method are arc discharge, laser ablation and acidic oxidation (Wang et al., 2019). The bottom-up approach implies carbonization with supported route (Baker & Baker, 2010). The carbonization is the conversion of organic matter into carbon by heating it to a high temperature in the absence of air or in presence of low amounts of other reagents, solvents, or catalysts. The supported route means utilization of supports to localize the growth of CDs by blocking agglomeration of nanoparticles during treatment with high temperature (Liu et al., 2009). Some examples of bottom-up method are combustion routes, microwave pyrolysis, electrochemistry method and hydrothermal synthesis (Wang et al., 2019). I am going to focus on the hydrothermal synthesis method, because it was used by my supervisor to produce CDs.

Hydrothermal synthesis is one of the most commonly used methods in synthesis of CDs, because of the simple setup and almost uniform size and high quantum yield (QY) of outcome particles (Shen et al., 2012). The QY is the ratio of the number of emitted photons to the number of absorbed photons. It is used to measure efficiency of photon emission through fluorescence. The higher QY means the brighter fluorophore and the stronger fluorescence signal intensity (Lakowicz, 2010). The principle of hydrothermal method is that small organic molecules, polymers or natural sources like grass, orange juice or beetroot extract, are dissolved in water or in organic solvent to form the precursor of reaction. Then it is transferred to Teflon-lined stainless-steel autoclave. The reaction precursors are then treated with high temperature for several hours. This merges the precursors into carbon seeding cores which then grow into CDs with the size up to 50 nm (Anwar et al., 2019). After that product is centrifuged and filtered to obtain pure nanoparticles. The QY can be up to 80% which is almost equal to fluorescent dyes (Zhu et al., 2013). The composition of CDs can be controlled by choosing appropriate precursors. Schematic representation of hydrothermal method can be seen on figure 2. Thus, doping with different heteroatoms and further enhancement in certain characteristics is possible. In addition, this method is easy and can be a promising approach in design and production of novel CDs with various properties.

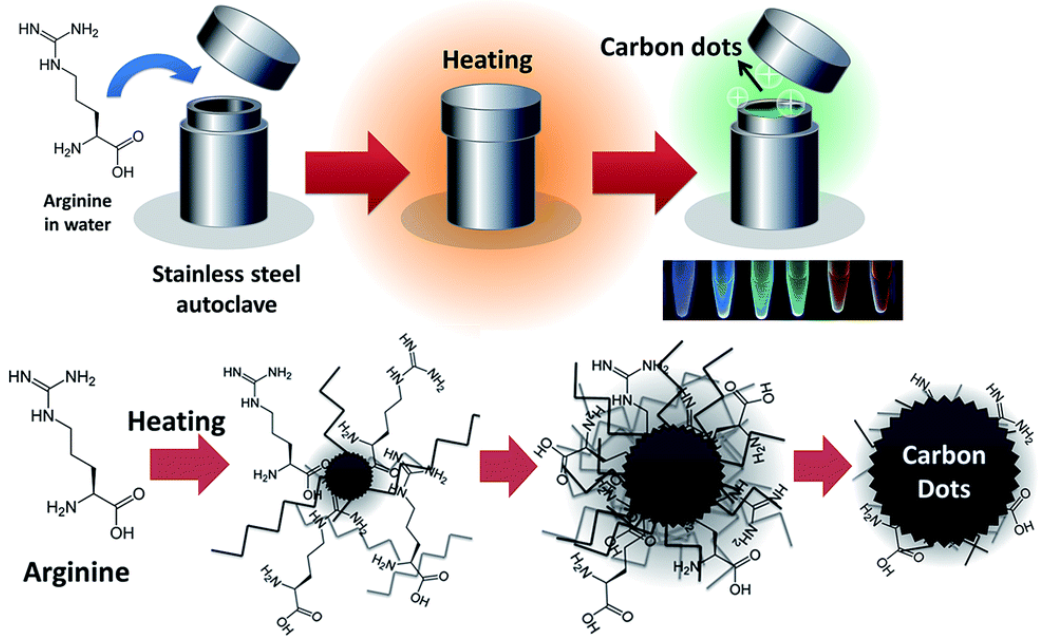

Figure 2. Hydrothermal method scheme with arginine as reaction precursor. Adapted from *Pseudo-multicolor carbon dots emission and the dilution-induced reversible fluorescence shift* by Y-C.Chen, C-Y. Nien, K.Albert, C-C.Wen, Y-Z.Hsieh and H-Y.Hsu, 2016, *Royal Society of Chemistry Advances, 6,* 44024-44028

1.1.2 Properties

Because of different chemical groups on the surface and spherical structure, CDs exhibit following properties: absorbance, photoluminescence (PL), chemiluminescence, electrochemical luminescence, enzyme mimetic activity as well as antibacterial and anticancer properties.

CDs usually show optical absorption in the UV region and have an absorption band at around 260-320 nm. The wavelength can be controlled by proper surface passivation of CDs (Miao et al., 2015). Also, CDs are able to emit different wavelengths by PL. The color can be controlled by the size and surface groups of CDs (Li et al, 2012). Thus, CDs passivated with polyethyleneimine showed blue, green, or red luminescence when excited under ultraviolet (330-385 nm), blue (460-495 nm), or green (530-550 nm), respectively (Liu et al., 2012). Chemiluminescence and electrochemical luminescence are also important properties of CDs. These are used in biosensing and bioimaging.

For the antibacterial properties some CDs were able to completely or partially inhibit colony formation in certain bacterial species. The effectiveness of inhibition of growth depended on the source from which CDs were synthesized, functionalization and doping with certain elements and chemical groups, and whether CDs were exposed to irradiation or not (usually with ultraviolet light). In the simplest form, Li et al. produced CDs from vitamin C and tested

them on Gram-positive *Staphylococcus aureus* and *Bacillus subtilis*, and Gram-negative *Bacillus* sp. WL-6 and *Escherichia coli*. It was found that a concentration of 50 μg/ml was able to completely inhibit colony formation in *Bacillus* species, while for *E. coli* and *S. aureus* concentration of 100 μg/ml was required. In addition, the authors studied the mechanism of bacterial growth inhibition. They found out that CDs can bind to membrane and can be internalized by diffusion. CDs bound to cell membrane lead to isolation from growth medium and leakage of intracellular components, whereas internalized CDs can bind to DNA and RNA via noncovalent bond and cause loosening and unwinding of nucleic acids (Li et al., 2018). In another study conducted by Jian et al. CNDs were synthesized from three biogenic polyamines: putrescine, spermidine, and spermine. They found out that pure spermidine and spermidine-derived CDs showed antibacterial activity against nonmultidrug-resistant *E. coli*, *S. aureus*, *Pseudomonas aeruginosa*, *Salmonella enteritidis*, and against methicillin-resistant *S. aureus*. The minimum inhibitory concentration of spermidine-derived CDs was approximately 2500 times lower than that of spermidine. The main mechanism of antibacterial activity was through binding to phospholipids, porins and peptidoglycans causing membrane destabilization. The high level of binding was due to "ultra-high" positive charge of CDs. In addition, CDs were able to bind to DNA and siRNA, thus, interrupting processes like gene expression and duplication (Jian et al., 2017). Travlou et al. conducted a study in which they doped CDs with either nitrogen or sulfur, and tested their antibacterial effect on *Bacillus subtilis* and *E. coli*. It was found that both CDs showed higher affinity to *B. subtilis* than to *E. coli*. Also, nitrogen-doped CDs were more efficient that sulfur-doped ones. This was due to the positive surface charge and better ability to produce reactive oxygen species (ROS) in aqueous solutions. The inhibition of bacterial growth of sulfur-doped CDs was shown to be size-dependent, because their negative surface charge is not favorable for interactions with cell membrane (Travlou et al., 2018). Furthermore, it was shown by Chatzimitakos et al., that co-doping CDs with nitrogen and sulfur produces better growth inhibitory effect than from CDs doped with only N or S (Chatzimitakos et al., 2020). In order to increase the antibacterial effect of CDs or to achieve several effects simultaneously, like antibacterial with gene transfection or antibacterial with bacterial differentiation, different molecules or other nanoparticles were used to functionalize CDs. Thus, Dou et al. performed functionalization of CDs with linear and branched poly(ethyleneimine). It was used because it shows good permeabilization against Gram-negative bacteria, and it is widely used as a gene transfection agent. After functionalization and treatment of bacteria, the recorded minimum inhibitory concentration for *S. aureus* was 50% lower for linear poly(ethyleneimine) compared with branched one. This was due to two

reasons: (1) linear poly(ethyleneimine) can cause depolarization of the membrane of *S. aureus*; (2) it has better permeabilization properties than branched one. However, branched poly(ethyleneimine) was better at gene transfection properties than linear one (Dou et al., 2015). Thus, CDs can have various antibacterial mechanisms such as binding to cell wall and isolation from growth medium, internalization and binding to DNA and RNA and production of ROS which then leads to oxidative stress. Hereby, antibacterial properties of CDs depend on various factors such as charge, size, doping with heteroatoms, and functionalization with different molecules, and require proper control of synthesis in order to achieve desired result. This area is still emerging and requires more experiments and trials.

Besides antibacterial properties, CDs also have anticancer properties or can be used in targeting tumor cells and delivering drugs. Several studies were conducted on various cancer cell lines. Almost all of them indicate that there is certain degree of growth inhibition in certain cancer cell lines. Thus, Sawant & Bamane produced CDs from ginger by hydrothermal method and subsequently exposed MCF-7 breast cancer cells with them. They used 5-fluorouracil (5-FU) drug as a positive control. As a result, CDs decreased cell viability of MCF-7 up to 64% at concentration of 5 μg/ml, and up to 78% at 10 μg/ml compared to 5-FU, which showed inhibition to 15% at 5 μg/ml and 19% at 10 μg/ml. The CDs that they synthesized had antioxidant and reducing properties, as well as they contained free mobile electrons. These properties allowed them to produce ROS inside cells and thus inhibit growth (Sawant & Bamane, 2016). In similar study, done by Li et al., researchers also produced CDs from ginger and treated A549 (human lung cancer), MDA-MB-231 (human breast cancer), HeLa (human cervical cancer), HepG2 (hepatocellular carcinoma), and MCF-10A (normal mammary epithelial) cell lines with them. The results showed that gradual increase in dose does not affected MCF-10, A549 and HeLa cells. However, there was decrease in viability of HepG2 cells upon increasing dose of CDs from 0 to 2.8 mg/ml. Furthermore, CDs induced cytotoxicity to MDA-MB-231 cells when their concentration was higher than 1.4 mg/ml. Also, they tested FL83B (mouse liver) cell line for viability, and no significant decrease in viability was observed upon exposure to CDs at doses ranging from 0 to 2.8 mg/ml. Further, researchers studied how CDs induce cell death in HepG2 cells. It was found that CDs are internalized by receptor-mediated and/or non-receptor-mediated endocytosis and mostly reside in the cytoplasm. Here, they generate ROS, which leads to oxidative stress and then to apoptosis (Li et al., 2014). Compared to tumor cells, toxicity of CCDs was also studied on normal cells, or, to be more precise, on standard mouse fibroblast cells line (NIH/3T3). It was found that toxicity depends on charge of CDs. Thus, neutral CDs are the safest ones because they did not cause

any abnormalities in morphology and cell cycle up to doses of 30 µg/ml. Negatively charged CDs affected the cell cycle and induced higher oxidative stress than neutral ones. Positively charged CDs were the most cytotoxic. They entered the cell nucleus and caused largest changes in cell cycle (Havrdova et al., 2016). Hereby, CDs can be lethal to cancer cells because of their antioxidant and reducing properties.

Another important property of CDs is the enzyme mimetic activity. Some CDs are able to catalyze certain reactions and thus can be used as a substitute of certain enzymes. Such CDs are called *nanozymes*, a term coined from *nanoparticles* and enzymes. One example of nanozyme-catalyzed reaction is peroxidase reaction. CDs have shown intrinsic peroxidase-like activity, which can be used to catalyze the oxidation of 3,3',5,5'-tetramethylbenzidine (TMB), *o*-phenylenediamine (OPD) and 1,2,3-trihydroxybenzene (THB), producing typical color reactions (Garg & Bisht, 2016). It was found that the catalytic mechanism was due to increase in electron density and mobility in the CDs because of the electron transfer from TMB to CDs. This leads to acceleration of electron transfer from CDs to H_2O_2 and thus increase in the rate of TMB oxidation (Shi et al, 2011). Like enzymes, activity of CDs depends on pH, temperature and substrate concentration. The maximum catalytic activity of CDs was observed under following conditions: pH 3.5, 35 °C and 300 mM H_2O_2. Furthermore, CDs exhibited a ping-pong mechanism like in horseradish peroxidase. In addition, CDs displayed higher affinities to H_2O_2 and other peroxidase substrates than peroxidase enzymes (Shi et al, 2011). Thus, density and mobility of electrons of CDs can be studied in other types of reactions like, in this case, phosphatase reaction.

1.1.3 Applications

Firstly, CDs are used as biosensors. Because of their excellent PL properties, they are used for fluorescence analysis of different targets starting from small molecules like ions and H_2O_2, and ending with macromolecules like proteins. One example is the detection of mercury ions. These are heavy metal ions which cause contamination of the environment, can accumulate in vital organs and tissues, and may lead to development of different diseases. In one study Qin et al., prepared CDs from flour and determined that their PL was dependent on the binding of Hg^{2+} with detection limit of 0.5 nM (Qin et al., 2013). Another example is the detection of H_2O_2. H_2O_2 is involved in cell proliferation, signal transduction, aging and death. Nonetheless, lots of H_2O_2 can harm the central nervous system and cause various diseases. Liu et al., produced the system of CD-catalyzed silver nanoparticles and nitrogen-doped CDs. This system was able to selectively monitor H_2O_2 levels with detection limit of 0.5 µM (Liu et al., 2014). Yet another example is the detection of thrombin. Thrombin is a specific serine endoprotease and it acts as

the key enzyme in pathological processes. It contains multiple sites for binding of aptamers. Aptamers are artificial single-stranded DNA or RNA that target different analytes with high affinity. Xu et al., were able to design CDs modified with aptamers which were able detect thrombin levels with the detection limit of 1 nM (Xu et al., 2012).

Secondly, CDs are used in bioimaging. High stability, bright fluorescence, excellent water solubility and controlled cytotoxicity are key factors in this. One example is CDs produced by Na et al. that emit luminescence at 450 nm which are used for imaging of human serum proteins on gels. After the polyacrylamide gel electrophoresis procedure, the proteins were stained by directly incubating with an acetic acid diluted CD solution. This method provided simple staining steps and high resolution (Na et al., 2013). Another example is the LLC-PK1 cell imaging. CDs were internalized by endocytosis and green fluorescence was detected. The cells were highly viable which confirms the low toxicity of nanoparticles (Hsu et al., 2012).

Thirdly, CDs are being tested in drug delivery. They are good candidates for this, because of their rapid cellular uptake, excellent biocompatibility, bright photoluminescence, high stability, and, most importantly, limited influence of drug activity. He et al. combined CDs with metal-organic framework to carry pH-responsive drug, 5-fluorouracil, to cancer cells. Different release efficiencies were observed in neutral and acidic environments. Overall, pharmacological activity of the drug was satisfactory, demonstrating that CDs have potential to be used in biomedical delivery platform (He et al., 2014).

1.1.4 Characterization

Several methods are used to characterize CDs. These are: three microscopy methods which include Scanning Electron Microscopy (SEM), Transmission Electron Microscopy (TEM) and High-Resolution Atomic Force Microscopy (HR-AFM), and, two spectroscopy methods that are Ultraviolet-visible Spectroscopy (UV-vis) and Fourier-Transform Infrared Spectroscopy (FT-IR).

SEM is a type of electron microscopy in which an image of CDs is produced by continuous scanning of the surface of sample with a focused beam of electrons. The atoms of the sample interact with upcoming electrons and thus, the image of surface is created. TEM is also a type of electron microscopy where electrons are transmitted through the sample, and the image is formed based on the electron transmission of CDs. Here, however, image of the whole specimen is generated, instead of only surface like in SEM. TEM is used when there is need in higher resolving power than in SEM. Both SEM and TEM are used to detect morphology, size distribution and particle size of CDs. Also, these methods are used to determine whether there

is agglomeration or dispersion of particles present. The diameter of CDs is estimated by randomly counting the size of particles on TEM images, and then taking the average (Xu et al., 2014).

HR-AFM is a type of scanning probe microscopy. Here, images are formed by continuous scanning of specimen by a physical probe. Thus, the data is collected by very precise "touching" the sample. Then, as its name suggests, very high-resolution images are generated. Unlike SEM and TEM, AFM is not only able to produce 2D images of CDs, but also can generate 3D information about the morphology of surface of CDs (Xu et al., 2014).

UV-vis is a type of absorption spectroscopy techniques. The aim of this technique is to measure how much light is being absorbed by sample at each wavelength. In UV-vis, firstly, the sample is illuminated by a monochromatic light beam, then, there is measurement of how much light is absorbed, after that, steps are repeated for each wavelength. Thus, UV-vis spectrum of CDs is obtained. It was found that all types of CDs absorb light in UV-vis region of electromagnetic spectrum. UV-vis technique is also used to determine which wavelengths are emitted by CDs. In addition, together with PL Spectroscopy, UV-vis can be used to detect QY of CDs (Xu et al., 2014).

FT-IR is a technique similar to UV-vis. Here, however, instead of using one wavelength at a time, a beam containing various frequencies of light is shined. Then, there is measurement of how much of that light beam is being absorbed by specimen. After that, next beam with different combination of frequencies is shined at sample and the process repeats. In the end, a program analyzes all data and determines absorption at each wavelength. FT-IR is used to identify which functional groups are present in CDs. Thus, hydroxyl and carbonyl groups can be detected by FT-IR. Furthermore, this technique is used to investigate the presence of doped heteroatoms. In this way, amide/amine, alkyl sulfide, phosphates, boronic acid and organosiloxane groups are detected on the surface of CDs, stating that nitrogen, sulfur, phosphorus, born, and phosphorus atoms were successfully integrated into the structure of CDs (Xu et al., 2014).

1.2 Alkaline Phosphatase

Alkaline Phosphatase (ALP) is an enzyme involved in the hydrolysis of phosphate-containing compounds. As its name suggests, ALPs optimum pH is alkaline. ALP is bound to membrane via a glycosyl phosphatidyl inositol anchor and functions as an ectoenzyme. It is found in almost all living organisms, starting from bacteria and ending with human. In bacteria its main

function is to transfer inorganic phosphate (P_i) during its shortage. In human it is mainly involved in liver metabolism and skeleton development (Buchet et al., 2013). The level of ALP in blood is used to detect various diseases. This procedure is called ALP test and it usually detects abnormal levels of ALP in blood which can be caused by disturbances in liver, bones or gall bladder.

1.2.1 Isoforms of ALP

There are four isoforms of ALP which are encoded by four structural genes. The isoenzymes are divided into two categories: tissue-nonspecific ALP (TNALP) and tissue-specific ALPs (TSALPs). There is only one TNALP and it has the same name. TNALP is expressed in a wide variety of regions such as bone, liver, kidney, developing nervous system and neutrophils. It is mainly involved in skeletal mineralization because it supplies with free inorganic phosphate (P_i) which is essential for bone mineral and teeth matrix. Moreover, TNALP is involved in vitamin B6 metabolism and thus in the metabolism of an important neurotransmitter – γ-aminobutyric acid. (Haarhaus et al., 2017). For TSALPs, there are three isoenzymes. These are intestinal alkaline phosphatase (IALP; Kasahara isoenzyme), placental alkaline phosphatase (PALP; Regan isoenzyme), and germ cell alkaline phosphatase (GCALP; Nagao isoenzyme). Their names tell for the sites of their expression. The GCALP is expressed by embryonic cells and carcinoma cells. PALP is only found in primates. It allows maternal immunoglobulin G to pass through placenta, and generally improves the development and growth of embryos by an unknown mechanism (Štefková et al., 2015). The function of GCALP is not known (Haarhaus et al., 2017), however high levels of GCALP and PLALP are used as markers of tumor diseases. Some of these tumor diseases are carcinoma of the gastrointestinal tract and uterus, squamous cell carcinoma of the lung, and germ cell tumors. IALPs role is to transport triglycerides and fatty acids from the intestine to the circulation. In addition, it controls the pH of the surface of duodenum and dephosphorylates the bacterial endotoxins in the colon thus detoxifying them (Štefková., 2015). In this research Calf Intestinal Alkaline Phosphatase was used as a positive control. In addition, in bacterial assays, *Escherichia coli* and *Lactococcus lactis* were tested for growth in solutions containing CDs. In *E. coli* there are three isoforms of ALP which are located mostly in periplasmic space and differ in the N-end of peptide chain, amount of arginine, and zinc and P_i content. The number of isoforms depends on the availability of inorganic substrate. Thus, when there is enough of P_i, only one isoform is present, and when the P_i is scarce – other two forms are being synthesized. All three isoforms show different activities, with the third form being the most active one and the first – the least active one. The

pH optimum for all three isoforms is 8.5 and all isoforms are inhibited in equal extent by P_i, a well-known competitive inhibitor of ALP. All isoforms hydrolyze broad range of substrates. Moreover, the first isoform is better at hydrolyzing ATP and inorganic pyrophosphate, whereas the third isoform better hydrolyzes polyphosphates (Nesmeyanova et al, 1981).

1.2.2 Phosphatase activity

ALP is a dimeric metalloenzyme that catalyzes the hydrolysis of phosphate esters. It exhibits three types of activity: hydrolytic, phosphotransferase and pyrophosphatase. By hydrolytic activity ALP is able to remove phosphate group by using water. Using phosphotransferase activity, it is able to transfer phosphate group to another alcohol. By pyrophosphatase activity ALP can split ester with two interconnected phosphates into two separate phosphate esters (Štefková et al., 2015). The general structure of ALP is as follows: it is a 2-fold symmetric dimer with two active sites that are located 30 Å from each other. The active site region consists of three amino acid residues – aspartic acid, serine and alanine, which have the following order: 101, 102 and 103 respectively. Ser102 is directly involved in phosphorylation and dephosphorylation. In addition to residues there is a, so called, metal triplet that consists of two Zn^{2+} and one Mg^{2+}. Also, there are Arg166 and other amino acid residues in a close proximity. Furthermore, there are several water molecules in the active site which form an extensive hydrogen-bonding network (Kim & Wyckoff, 1991). The structure of ALP can be seen on figure 3.

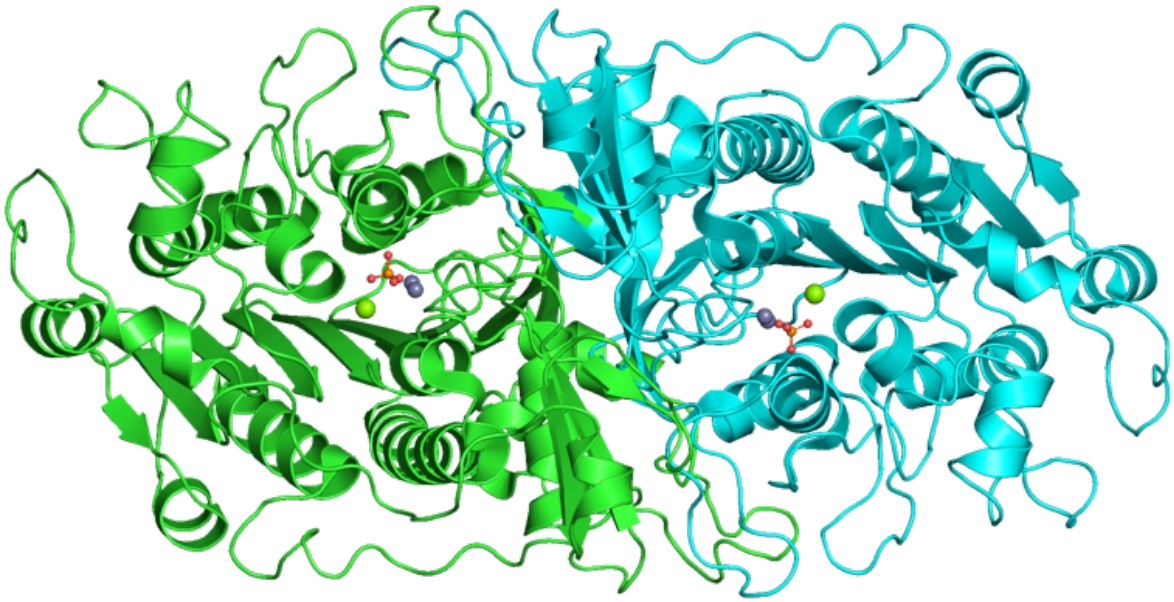

Figure 3. Three-dimensional structure of *E. coli* ALP. Monomer A is shown in green and monomer B is shown in cyan. Zinc ions are shown in grey, magnesium atom is shown in bright green, and phosphate ion is shown in orange. Adapted from https://www.ebi.ac.uk/pdbe/entry/pdb/1alk

It is well known that the most commonly phosphorylated amino acids are serine, threonine and tyrosine. ALP contains Ser102 in its active center and, its phosphatase activity is mainly due to this residue. The reaction mechanism is as follows: firstly, ALP approaches phosphate donor, R_1OP, and forms a non-covalent complex with it - $E \cdot R_1OP$ via pulling two side oxygen atoms by two Zn atoms in the active site. Secondly, oxygen atom of Ser102 attacks the phosphorus atom and forms the covalent bond with it. This creates a penta-co-ordinate intermediate – $E\text{-}R_1OP$. Thirdly, one of the Zn ions pulls electrons from phosphate group, thus allowing to the electrons in one of the P-O bonds to move to O atom of phosphate donor. After this step, ROH is released and phosphate group is now bound to O atom of Ser102. Then, the reaction can proceed in two ways, depending on the availability of phosphate acceptor. If there is no phosphate acceptor, then one Zn atoms covalently binds water molecule and allows the electrons from one of the O-H bonds to flow to phosphorus. At the same time, electrons from P-O with Ser102 flow to O atom of serine. Thus, phosphoseryl intermediate is hydrolyzed and P_i is released. In the second way, phosphate acceptor, R_2OH approaches, and as in the first way acts like water, but in the end accepts the phosphate group and becomes R_2OP (Kim & Wyckoff, 1991).

1.2.3 ALP in health and diseases

ALP is expressed at various sites of human organism and is involved in many essential processes that require P_i. Therefore, deficiency or excess of ALP can lead to development of various diseases, as well as it can be used as a marker of certain diseases. The activity of bone and liver ALPs in serum are routinely used to diagnose diseases associated with these organs. Serum of individuals of different ages is collected and analyzed for activity of each isoenzyme. It was shown that the data collected from healthy individuals suggests that the levels of bone ALP constitute about half the total ALP activity in adults. Thus, the normal range of serum ALP is 20 to 140U/L. If the levels exceed these numbers, then there is a disease of bone, liver or other organs. Elevated ALP levels can show that there is an active bone formation such as in case of Paget's disease of bone, or it can show presence of hyperparathyroidism, the disease that affects blood calcium level. In addition, it can show presence of damaged liver cells and vitamin D deficiency. Moreover, ALP levels are increased in people with untreated Celiac disease and it can be sign that the bile ducts are obstructed. Increased PLALP levels are observed during seminomas, cancer of ovaries, lung and gastrointestinal tract. Furthermore PLAPL and GCALP are highly expressed in cells taken from choriocarcinoma and breast cancer. Usually, ectopic expression of ALP is a sign of many human cancers. IALP, for

example, is highly expressed in hepatocellular carcinoma. Also, ALP levels are elevated during metastatic prostate cancer cells, compared to non-metastatic one (Sharma et al, 2013). Deficiency in ALP is less common than the excess. Nevertheless, it is associated with conditions such as, malnutrition, magnesium deficiency, chronic myelogenic leukemia, several types of anemia, Wilson's disease, men who recently received heart surgery and postmenopausal women who receive estrogen therapy due to osteoporosis. Also, oral contraceptives have shown to decrease ALP levels. Another important disease associated with deficiency in ALP is hypophosphatasia, a genetic disorder in which there is an abnormal metabolism of pyridoxal-5'-phosphate (the predominant form of vitamin B6). This leads to hypomineralization of teeth and skeleton, followed by rickets and loss of teeth or osteomalacia and dental problems in adults as a result of accumulation of inorganic pyrophosphate. Individuals with hypophosphatasia exhibit a missense mutation in TNALP gene and therefore have generalized deficiency of TNALP, despite the fact that PLAP and IALP activity levels are normal. Thus, with ALP being essential component of cellular processes such as protein phosphorylation, apoptosis, cellular and migration, it is a widely used marker of various diseases and health conditions (Sharma et al, 2013).

1.3 Enzyme kinetics

Sulfur doped CDs are hypothesized to have phosphatase activity because of the sulfur-containing groups. Sulfur doped CDs tend to aggregate into larger ring-like structures, with sulfur-containing groups pointing outwards. These structures are hypothesized to have dense and mobile electrons, like peroxidase mimicking CDs, which then participate in phosphatase reaction and this makes sulfur doped CDs act like biological enzymes. Therefore, to describe the reaction mechanism of CDs Michaelis-Menten model for enzyme kinetics and inhibition was used.

1.3.1 Michaelis-Menten model

Enzyme kinetics is a discipline about determination of the rate of reaction and how it changes in response to changes in experimental parameters. To determine the rate of reaction the Michaelis-Menten model is used. As it is written by Nelson in the book of Lehninger principles of biochemistry, this model states that a substrate S binds reversibly to enzyme E and forms enzyme-substrate complex ES, then this complex breaks down into free enzyme E and product P. The last step is assumed to be irreversible. The described system can be represented as follows:

$$E + S \leftrightharpoons ES \rightarrow E + P$$

After the step of converting the substrate into a product, catalyst E remains unchanged. In this case, sulfur doped CDs are believed to remain unchanged because of their rigid oligomer ring-like structure. Since the concentration of E is not changing, Michaelis-Menten model provides a relation of reaction to substrate concentration which is represented in the Michaelis-Menten equation itself:

$$v = \frac{V_{max}[S]}{K_m + [S]} \quad (1)$$

Here, v represents the initial rate of reaction, V_{max} represents the maximum rate of reaction, K_m is the substrate concentration at which v is half of V_{max}, in other words, it is called the Michaelis-Menten constant, and [S] is the concentration of substrate. The equation 1 creates a famous Michaelis-Menten plot which shows direct relation of reaction rate to substrate concentration. On this plot, the v increases with the increasing [S] and going towards V_{max}. However, it never reaches V_{max}, because at V_{max} enzyme is fully saturated with substrate and this never happens because enzyme needs to release the molecule of product and be available for next substrate molecule. In addition, this plot shows approximate K_m value, and this value is helpful in measuring the affinity of enzyme to substrate. Thus, high K_m indicates low affinity for substrate, and low K_m indicates high affinity for substrate. Enzymes with high K_m tend to saturate and accelerate the reaction rate slower than enzymes with low K_m (Nelson, 2013). Even though Michaelis-Menten plot gives information about reaction rate of enzyme, it is not linear and it is difficult to get the exact K_m and V_{max} values out of it. To do this, Lineweaver-Burk equation is used:

$$\frac{1}{V_0} = \frac{1}{V_{max}} + \frac{K_m}{V_{max}[S]} \quad (2)$$

This equation generates the Lineweaver-Burk plot in which the y-intercept equals to $1/V_{max}$, x-intercept equals to $-1/K_m$, and the slope of line equals to K_m / V_{max}. This plot makes it easier to define kinetic parameters. Also, it is more precise than simple Michaelis-Menten plot where kinetic parameters can only be approximated (Nelson, 2013). Based on the studies done on peroxidase-mimicking CDs, sulfur doped CDs are assumed to behave like catlysts and obey the rules described above (Garg & Bisht, 2016).

1.3.2 Inhibition

Enzyme inhibitors are the molecules that can interfere with catalysis, thus slowing or stopping the reactions. There are two types of inhibition: reversible and irreversible. In reversible one, the inhibitor binds an enzyme transiently and is able to detach from it. There are four types of reversible inhibitors:

1. Competitive inhibitors are the molecules that structurally resemble the substrate and thus can bind enzyme in the active site. P_i is an example of competitive inhibitor of ALP.
2. Uncompetitive inhibitors can only bind enzyme-substrate complex and thus can slow down the reaction rate.
3. Non-competitive inhibitors bind both enzyme and enzyme-substrate complex with equal affinity. Here, the binding of inhibitor reduces the activity of enzyme but not it's binding to substrate.
4. Mixed inhibitors can also bind to enzyme and enzyme-substrate complex. However, this type of inhibitors affects the enzyme's binding to substrate and vice versa.

In irreversible inhibition, a molecule binds to enzyme permanently, usually covalently, affects the structure of the active site, and, thus, prevents enzyme from catalyzing the reaction. Irreversible inhibitors can bind to either enzyme alone, or to enzyme-substrate complex (Nelson, 2013). It was found that peroxidase-mimicking CDs can be inhibited by azobenzene by binding to bind sites of TMB substrate (Lv et al., 2018). Based on this study my CDs are assumed to behave like catalysts in terms of inhibition and were tested for inhibition by copper metal ions because these are inhibitors of protein phosphatases.

2 MATERIAL AND METHODS

2.1 Reagents, buffers

Table 1. List of reagents and solutions

Name	Concentration or Composition	Source
Beetroot extract-derived sulfur doped carbon dots	0.05, 0.1, 0.2, 0.5 and 5 mg/ml	In house made
BCIP-NBT	2.5 mg/ml	Thermo Scientific™
pNPP	10 mM	Thermo Scientific™
Sulfur – 99.998% trace metals basis	Elemental sulfur in the form of powder	Sigma-Aldrich
Invitrogen™ Calf Intestinal Alkaline Phosphatase	20 U/µl, diluted in 1:400 proportion	Invitrogen™
pH 4.7 buffer	0.1 M CH_3COOH	In house made
pH 7 buffer	0.2 M $Na_2HPO_4•_2H_2O$	In house made
pH 8.5 buffer	0.1 Tris-HCl	In house made
Ethylenediamine	0.7 mM	In house made

Table 2. List of bacterial culture reagents

Name	Abbreviation	Company
LB Broth, Lennox	LB Broth	Fisher Chemical™
LB Agar, Miller	LB agar	Fisher Chemical™

Table 3. List of bacterial strains

Name	Usage	Company
Escherichia coli (Migula) Castellani and Chalmers (ATCC® 23735™)	Cultivation	ATCC®
Lactococcus lactis subsp. Lactis derived from ATCC® 19435™	Cultivation	Microbiologics Inc.

2.2 Synthesis of sulfur-doped CDs

2.2.1 Preparation

To prepare BTSCD, the dried beet powder was mixed with certain amount of ethylenediamine, sulfur, and distilled water. The mixture then underwent a hydrothermal reaction at 200ºC for 5 h. The liquid part was collected through filter after hydrothermal reaction. It was centrifuged to get rid of the insoluble particles. The liquid upon centrifuging was then placed in an oven at

60ºC. The dried BTSCD were used to perform FT-IR, SEM, TEM measurement, and to make the stock solution with the concentration of 5 mg/ml.

2.2.2 Hydrothermal method

The hydrothermal method implies the use of organic molecules, polymers or raw materials such as orange juice, grass, or, in this case, beetroot extract as precursors of reaction. The mixture obtained in the previous step was dissolved in 60 ml of dH_2O and placed in Teflon-lined autoclave. Hydrothermal treatment was done at 200ºC for 5 hours. Following that, liquid phase was collected and exposed to centrifugation at 10000 rpm for 10 minutes. The residue was collected and dialyzed against de-ionized water for two days. This step was done to remove unreacted reactants and molecular-like by-products, thus purifying the CDs. The CDs were then collected and diluted with dH_2O to desired concentration. This method was developed by Liu et al and was modified by Dr. Fan (Liu et al., 2018)

2.3 Characterization

2.3.1 Fluorescence spectroscopy

The fluorescence spectroscopy measurements were performed at the room temperature using Agilent Technologies Cary Eclipse Fluorescence Spectrophotometer at the 360 nm excitation wavelength. Three concentrations of BTSCD were tested: 0.05, 0.2 and 0.5 mg/ml. This was done to detect the suitable concentration for obtainment of fluorescence spectra and to observe whether there is aggregation or segregation of nanoparticles. Then measurements were done and graphs of fluorescence spectra were generated. The graphs were merged, saved and further analyzed for the fluorescent emission of CDs.

2.3.2 FT-IR

The FT-IR measurements were conducted at the room temperature using a ThermoScientific Nicolet IS5 FT-IR spectrometer on a diamond ATR with the resolution of 2 cm^{-1} over the range of 400-4000 cm^{-1}. There were two measurements, one for non-doped CDs and another for doped ones. 3.5 ml of each CDs with concentration of 5 mg/ml were put into cuvette. Then measurements were done and graphs of FT-IR spectra was generated. The graphs were merged, saved and further analyzed for the presence of chemical groups, N and S in the structure of BTSCD.

2.3.3 SEM

The samples were prepared by taking a drop of BTSCD solution with concentration of 5 mg/ml and mixing it with 10 µl of water on aluminium foil. The samples were left to dry for 3 hours. After that, they were brought to SE microscope. Observation and analysis of samples were done on Carl Zeiss SUPRA 55 Scanning Electron Microscope.

2.4 BCIP-NBT assay

This assay consists of three parts. The first two are pH and temperature screening where BTSCD were tested at various pH and temperature conditions to determine how it affects its phosphatase activity with BCIP-NBT. The last one is the determination of kinetic characteristics of BTSCD.

2.4.1 pH screening

This part was done according to Abcam ab83369 Alkaline Phosphatase Assay Kit (Colorimetric) protocol. This protocol was modified to be suitable for CDs (Abcam, 2020). The pH screening was done in Nunc™ MicroWell™ 96-Well, Nunclon Delta-Treated, Flat-Bottom Microplate, further denoted as microplate. Three buffers with following pH were used: 4.7, 7 and 8.5. This was done to mimic the biologically relevant pH conditions that occur in lysosomes, cytoplasm and mitochondria, respectively. The concentrations of BTSCD and BCIP-NBT were 5 mg/ml and 2.5 mg/ml. For positive control Invitrogen™ Calf Intestinal Alkaline Phosphatase with concentration of 20 units/µl was used. To save enough ALP, it was diluted in 1:400 proportion. For negative controls either BTSCD or BCIP-NBT was mixed with pH buffers and dH_2O, it was added to fill the rest of total volume. For screening 20 µl of BTSCD, 30 µl of pH buffer and 50 µl of BCIP-NBT were mixed with total volume of 100 µl per well. For positive control 20 µl of ALP, 30 µl of pH buffer and 50 µl of BCIP-NBT were mixed. For first negative control of BCIP-NBT 20 µl of dH_2O, 30 µl of pH buffer and 50 µl of BCIP-NBT were mixed. For second negative control of BTSCD 20 µl of BTSCD, 30 µl of pH buffer and 50 µl of dH_2O were mixed. For each pH buffer there were three replicates of reaction. Afterwards, microplate was incubated at 25°C for 60 minutes in the dark. Following incubation microplate was put into the Thermo Scientific Varioskan Flash multimode reader to measure optical densities (ODs) of obtained mixtures to see whether there was a reaction or not. Measurements were done at 590 nm wavelength because it is the absorbance of insoluble precipitate which is dark blue to purple in color. ODs were analyzed and used to make graph of relative activity (RA) of mixtures versus pH conditions.

2.4.2 Temperature screening

This part was done according to Thermo Scientific 1-Step™ NBT/BCIP protocol. This protocol was modified to be suitable for CDs (Thermo Scientific, 2020). The temperature screening was done in microplates and in 500 µl Eppendorf™ Snap-Cap Microcentrifuge Safe-Lock™ Tubes, further denoted as microtubes. CDs were tested in two biologically relevant temperature conditions: 25°C and 37°C. The concentrations of BTSCD and BCIP-NBT were 5 mg/ml and 2.5 mg/ml. For positive control Invitrogen™ Calf Intestinal Alkaline Phosphatase with concentration of 20 units/µl was used. To save enough ALP, it was diluted in 1:400 proportion. For negative controls either BTSCD or BCIP-NBT was mixed with pH buffers and dH_2O, it was added to fill the rest of total volume. To ensure maximal performance of ALP and BTSCD pH 8.5 and 7 buffers were used, respectively. pH 7 buffer was also used in negative controls testing. 37°C screening was done in microtubes in order to transfer them into incubator and 25°C screening was done in microplate. For screening 20 µl of BTSCD, 30 µl of pH 7 buffer and 50 µl of BCIP-NBT were mixed with total volume of 100 µl per well or microtube. For positive control 20 µl of ALP, 30 µl of pH 8.5 buffer and 50 µl of BCIP-NBT were mixed. For first negative control of BCIP-NBT 20 µl of dH_2O, 30 µl of pH 7 buffer and 50 µl of BCIP-NBT were mixed. For second negative control of BTSCD 20 µl of BTSCD, 30 µl of pH 7 buffer and 50 µl of dH_2O were mixed. For each temperature there were three replicates of reaction. Filled microtubes were incubated at 37°C in 5% CO_2 incubator for 60 minutes in the dark. Microplate was incubated at 25°C for 60 minutes in the dark. Following incubation mixtures from microtubes were transferred to microplate and it was put into the microplate reader to measure ODs. Measurements were done at 590 nm wavelength. ODs were analyzed and used to make graph of relative activity (RA) of mixtures versus temperature conditions.

2.4.3 Kinetics of phosphatase activity

This part was done according to Rob L. Dean's protocol for kinetic studies with alkaline phosphatase in the presence and absence of inhibitors and divalent cations. This protocol was modified to be suitable for CDs and ALP (Dean, 2002). The experiment was performed in microplates. pH 7 buffer for BTSCD and pH 8.5 for ALP was used. For control Invitrogen™ Calf Intestinal Alkaline Phosphatase with concentration of 20 units/µl was used. To save enough ALP, it was diluted in 1:400 proportion. The concentrations of BTSCD and BCIP-NBT were 5 mg/ml and 2.5 mg/ml. To determine kinetic characteristics of BTSCD and ALP, there was gradual increase in concentration and volume of BCIP-NBT with gradual decrease in volume of pH 7/pH 8.5 buffer. Thus, with this gradient, and measurement of OD in time it was

possible to calculate rate of reaction and determine K_m and V_{max}. The reagents were added in following volumes shown in table 4:

Table 4. Volumes of reagents in kinetics assay

BTSCD/ALP (µl)	20	20	20	20	20	20	20	20	20	20	20	20
pH buffer (µl)	80	78.5	77	75.5	74	72.5	71	67	63	59	55	50
BCIP-NBT (µl)	0	1.5	3	4.5	6	7.5	9	13	17	21	25	30

For each BCIP-NBT volume there were three replicates of reaction. After mixing of all reagents, microplate was put into microplate reader to measure ODs. There were 16 steps of measurement. For BTSCD each step was 2 minutes long with 30 minutes in total, and for ALP first three steps were 2 minutes long and the rest thirteen steps were 4 minutes long with 54 minutes in total. This was done to fit ALP's performance and obtain reliable data points. Measurements was done at 590 nm wavelength at 25°C in the dark. After this, ODs were analyzed and used to make Michaelis-Menten and Lineweaver-Burk plots and determine K_m and V_{max}.

2.5 pNPP assay

This assay consists of three parts. The first two are pH and temperature screening where BTSCD was tested at various pH and temperature conditions to determine how it affects its phosphatase activity with pNPP. The last one is the screening for inhibition of BTSCD and ALP by Cu^{2+} ions.

2.5.1 pH screening

This part was done according to Thermo Scientific 1-Step PNPP protocol. This protocol was modified to be suitable for CDs (Thermo Scientific, 2020). The pH screening was done in microplate. Three buffers with following pH were used: 4.7, 7 and 8.5. The concentrations of BTSCD and pNPP were 5 mg/ml and 10 mM. For positive control ALP with concentration of 20 U/µl and in 1:400 dilution was used. For negative controls either BTSCD or pNPP was mixed with pH buffers and DH_2O, it was added to fill the rest of total volume. For screening 20 µl of BTSCD, 30 µl of pH buffer and 50 µl of pNPP were mixed with total volume of 100 µl per well. For positive control 20 µl of ALP, 30 µl of pH buffer and 50 µl of pNPP were mixed. For first negative control of pNPP 20 µl of DH_2O, 30 µl of pH buffer and 50 µl of pNPP were mixed. For second negative control of BTSCD 20 µl of BTSCD, 30 µl of pH buffer and 50 µl of DH_2O were mixed. For each pH buffer there were three replicates of reaction.

Afterwards, microplate was incubated at 25°C for 60 minutes in the dark. Following incubation microplate was put into the microplate reader to measure ODs of obtained mixtures to see whether there was a reaction or not. Measurements were done at 405 nm wavelength because it is the absorbance of para-Nitrophenyl product which is bright yellow in color and was formed due to cleavage of phosphate group. ODs were analyzed and used to make graph of RA of mixtures versus pH conditions.

2.5.2 Temperature screening

This part was done according to Thermo Scientific 1-Step pNPP protocol. This protocol was modified to be suitable for CDs (Thermo Scientific, 2020). The temperature screening was done in microplates and in 500 µl microtubes. CDs were tested in two biologically relevant temperature conditions: 25°C and 37°C. The concentrations of BTSCD and pNPP were 5 mg/ml and 10 mM. For positive control ALP with concentration of 20 U/µl and in 1:400 dilution was used. For negative controls either BTSCD or pNPP was mixed with pH buffers and DH_2O, it was added to fill the rest of total volume. To ensure maximal performance of ALP and BTSCD pH 8.5 and 7 buffers were used, respectively. pH 7 buffer was also used in negative controls testing. 37°C screening was done in microtubes in order to transfer them into incubator and 25°C screening was done in microplate. For screening 20 µl of BTSCD, 30 µl of pH 7 buffer and 50 µl of pNPP were mixed with total volume of 100 µl per well or microtube. For positive control 20 µl of ALP, 30 µl of pH 8.5 buffer and 50 µl of pNPP were mixed. For first negative control of pNPP 20 µl of DH_2O, 30 µl of pH 7 buffer and 50 µl of pNPP were mixed. For second negative control of BTSCD 20 µl of BTSCD, 30 µl of pH 7 buffer and 50 µl of DH_2O were mixed. For each temperature there were three replicates of reaction. Filled microtubes were incubated at 37°C in 5% CO_2 incubator for 60 minutes in the dark. Microplate was incubated at 25°C for 60 minutes in the dark. Following incubation mixtures from microtubes were transferred to microplate and it was put into the microplate reader to measure ODs. Measurements were done at 405 nm wavelength. ODs were analyzed and used to make graph of RA of mixtures versus temperature conditions.

2.5.3 Inhibition screening

This part was done to see if there is any inhibition of phosphatase activity of BTSCD or ALP by copper ions. It was done according to Rob L. Dean's protocol for kinetic studies with alkaline phosphatase in the presence and absence of inhibitors and divalent cations. This protocol was modified to be suitable for CDs (Dean R, 2006). The screening was performed

in microplate. As in pH screening, three buffers with following pH were used: 4.7, 7 and 8.5. This was done to see if there is any inhibition at biologically relevant pH conditions. The concentrations of BTSCD and pNPP were 5 mg/ml and 10 mM. ALP's concentration was 20 units/µl and it was diluted in 1:400 proportion to save enough ALP. For screening 20 µl of BTSCD or ALP, 30 µl of pH buffer, 50 µl of pNPP and 10 µl of Cu^{2+} were mixed with total volume of 110 µl per well. For controls 20 µl of BTSCD or ALP, 30 µl of pH buffer and 50 µl of pNPP and were mixed. For each reaction there were three replicates. Afterwards, microplate was incubated at 25 °C for 60 minutes in the dark. Following incubation microplate was put into microplate reader to measure ODs of obtained mixtures to see whether there was inhibition or not. Measurements were done at 405 nm wavelength. ODs were analyzed and used to make graph of RA of mixtures versus pH conditions.

2.6 Bacterial growth assay

This assay was done to see if there is any inhibition or promotion of growth of *E. coli* and *L. lactis* by BTSCD.

2.6.1 *E. coli* screening

This part was done according to Culture of *E. coli* Microbial Growth Protocol and modified for use with BTSCD (Merck, 2020). First of all, bacteria were refreshed. This was done by taking 1 ml of stock bacterial solution and mixing it with 9 ml of LB Broth. LB Broth was prepared by taking 20 grams of LB Broth powder and dissolving it in 1 L of DH2O. The mixture of bacteria with LB Broth was left overnight for incubation in shaker at 37°C. Secondly, LB Agar was prepared from Lennox LB Agar powder by taking 12 grams and mixing it with 1 L of DH_2O in 1L bottle. The bottle was then placed into autoclave for 2.5 hours until complete dissolution of powder and sterilization of bottle. Afterwards, prepared LB Agar was poured into Petri dishes in a volume of approximately 15 ml until the half of the dish was filled. Petri dishes were placed in the hood under the UV light and left until LB Agar solidifies.

Next, 1:10000 dilution of *E. coli* was prepared in 1.5 ml Eppendorf™ Snap-Cap Microcentrifuge Safe-Lock™ Tubes, further denoted as tubes. Firstly, 1:100 dilution was prepared by taking 10 µl from original culture and mixing it with 990 µl of DH_2O in tube. Secondly, 1:1000 dilution was prepared by taking 100 µl from 1:100 dilution and mixing it with 900 µl of DH_2O in the next tube. Thirdly, 1:10000 dilution was prepared by taking 100 µl from 1:1000 dilution and mixing it with 900 µl of dH_2O in the next tube. 1:10000 dilution was used in this experiment because it is the most optimal dilution to observe the dose dependent

inhibition of growth by BTSCD. It was found by repetitive screening of 1:1000, 1:10000 and 1:100000 dilutions by the same procedure as written here.

Following that, mixtures of bacteria were prepared by mixing BTSCD, double distilled water (DDH_2O), LB Broth and *E. coli* itself in 1.5 ml tube. Two concentrations of BTSCD were tested, 0.1 mg/ml and 0.5 mg/ml because, again, it was found by repetitive screening, that these concentrations are optimal for detecting dose dependent inhibition of growth of *E. coli*. In addition, ALP was tested in the same manner with following dilutions: 1:400 and 1:1000. The reagents were mixed in volumes shown in table 5.

Table 5. Volumes of reagents for bacterial growth inhibition by BTSCD

Number	BTSCD/ALP (µl)	ddH_2O (µl)	LB Broth (µl)	Bacteria (µl)
1	0	160	140	500
2	8	152	140	500
3	40	120	140	500
4	80	80	140	500
5	160	0	140	500

The total volume in each tube was maintained at 800 µl. Numbers correspond to increasing stock volume and total concentration of BTSCD/ALP. LB Broth and ddH_2O make mixture with pH at about 6.5 which is close optimum pH of BTSCD – 7. Then, tubes were incubated for 3.5 hours at 37°C shaker. During incubation, Petri dishes with solidified agar were prepared for bacterial culture by marking five regions corresponding to numbers in table 5. Following incubation, mixtures were spread onto Petri dishes on areas with appropriate number. It was done by taking 4 µl from tube and placing three drops on area. These drops were spread via plastic inoculation loop by streaking method. For each number there were three replicates in total yielding three Petri dishes for each concentration of BTSCD. In the end, all dishes were sealed with parafilm and put into 5% CO_2 37°C incubator overnight. Next day, dishes were collected and analyzed. Colony forming units (CFUs) were counted manually and counting data was used to make graphs of dose dependent growth inhibition/promotion with the relation of the number of CFUs to the volume of BTSCD.

2.6.2 *L. lactis* screening

This part was done by the same method as in 2.6.1 but without ALP testing.

2.7 Statistical analysis

All of the statistical analysis was performed in Microsoft Excel 2019. For the pH, temperature and inhibition assays the RA was calculated in the following manner. For each reaction three replicate ODs were used to calculate the mean value. Following that, the highest mean was selected and all OD measurements were divided by that mean and multiplied by 100 to obtain percentage. From these percentages, again, mean was calculated and was used to make graphs. Standard deviation and Student's t-test were calculated also based on those means. Significant difference was defined by $p < 0.05$.

For the kinetics of phosphatase activity OD measurements for each time point were organized for each concentration of BCIP-NBT. Thus, there were 12 concentration points with 16 time points in each one. Three replicate ODs of reaction were used to calculate mean for each time point and for each concentration. These means were used to make scatter plots of time versus OD for each concentration point. On these plots there was determination of equation for trendline. The formula of trendline was as follows: $y = ax + b$, where a is the value of speed. Thereby, each speed value was obtained for each concentration. Then, using all speed and BCIP-NBT concentration values, Michaelis-Menten plot was generated. In addition, by using all speed and concentration values and taking them into the power of -1, 1/V and 1/[S] values were obtained and used to generate Lineweaver-Burk plot. Using this plot, the equation of trendline was obtained. The formula of equation is as follows: $y = kx + b$, where $k = K_m/V_{max}$ and $b = 1/V_{max}$. The values of K_m and V_{max} were calculated from obtained k and b coefficients.

For the bacterial growth assay three replicates for each concentration of BTSCD were used to calculate mean. The bar charts were generated based on these means. Standard deviation and Student's t-test were calculated also based on these means. Significant difference was defined by $p < 0.05$.

3 AIMS OF THE THESIS PROJECT

I. To develop and characterize sulfur doped carbon dots.

II. To check the phosphatase activity of the prepared carbon dots using para-Nitrophenyl Phosphate (pNPP) and 5-Bromo-4-chloro-3-indolyl phosphate-nitro blue tetrazolium liquid substrate system (BCIP-NBT) as substrates.

III. To determine kinetic characteristics of sulfur doped carbon dots.

IV. To detect the antimicrobial properties of the prepared carbon dots.

4 RESULTS

4.1 BTSCD fluoresce at 450 nm, contain C-S bond with amide groups and assemble into ring-shaped particles

4.1.1 Fluorescence spectroscopy

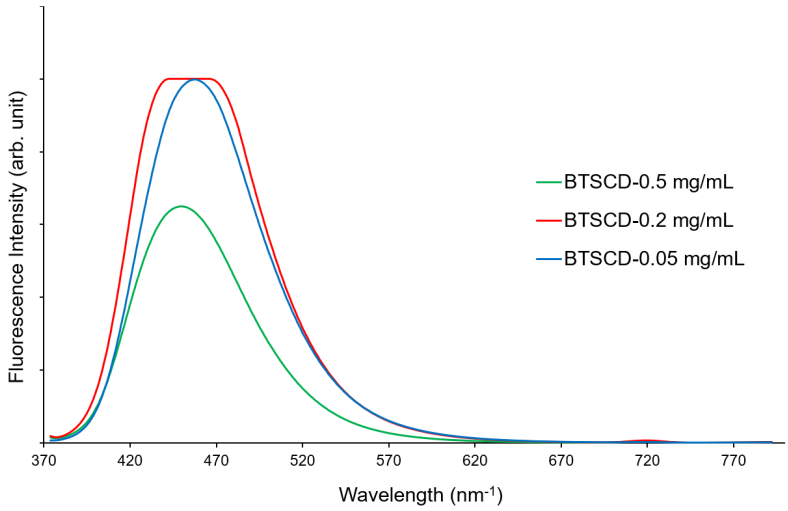

Figure 4. Fluorescence spectra of BTSCD at various concentrations.

4.1.2 FT-IR

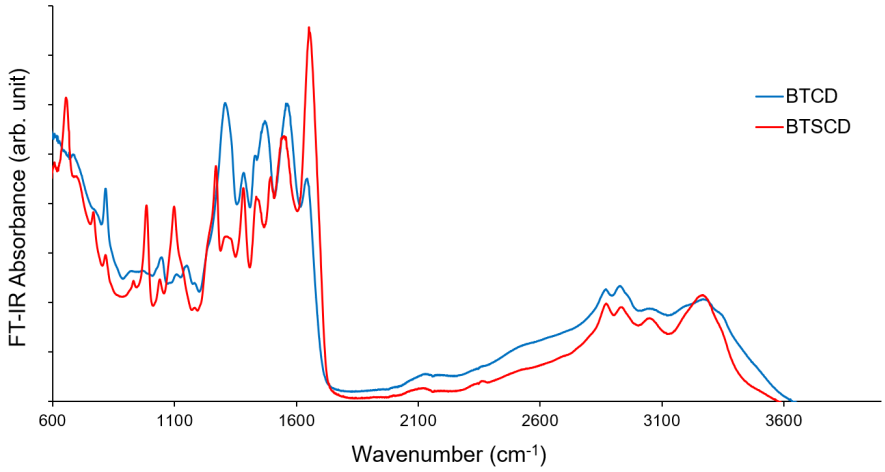

Figure 5. FT-IR spectra of beet-CDs and sulfur doped beet-CDs.

4.1.3 SEM

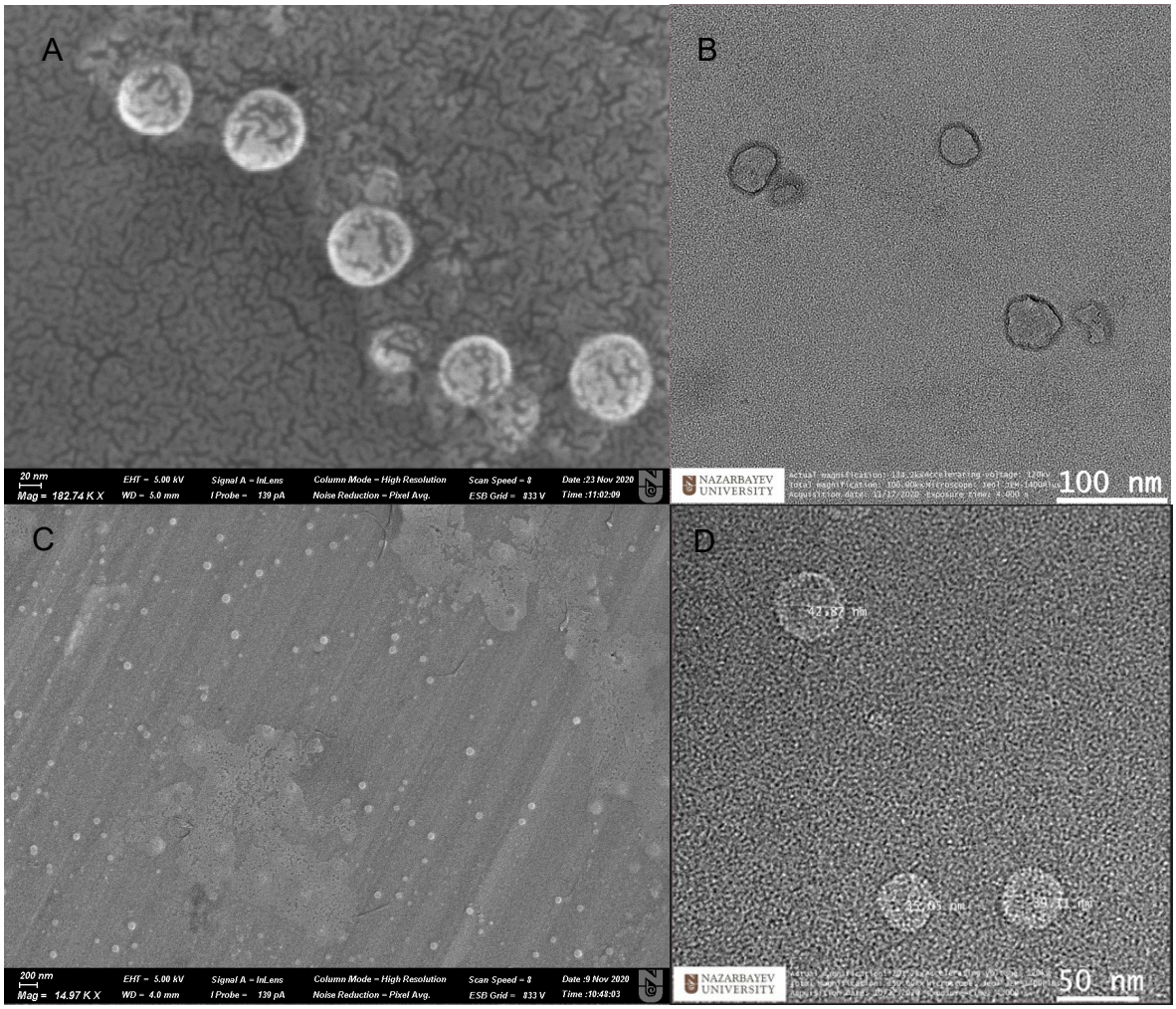

Figure 6. SEM images of BTSCD.

4.2 BTSCD exhibit high phosphatase activity with BCIP-NBT and high affinity to it

4.2.1 pH screening

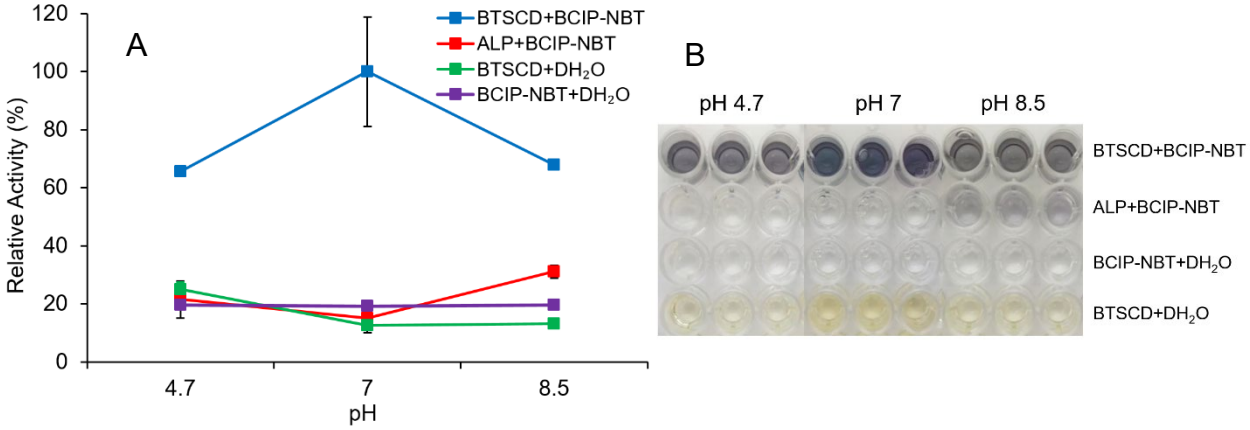

Figure 7. BTSCD pH assay with BCIP-NBT. (A) Relative activity of mixtures. (B) Wells after completion of reaction.

4.2.2 Temperature screening

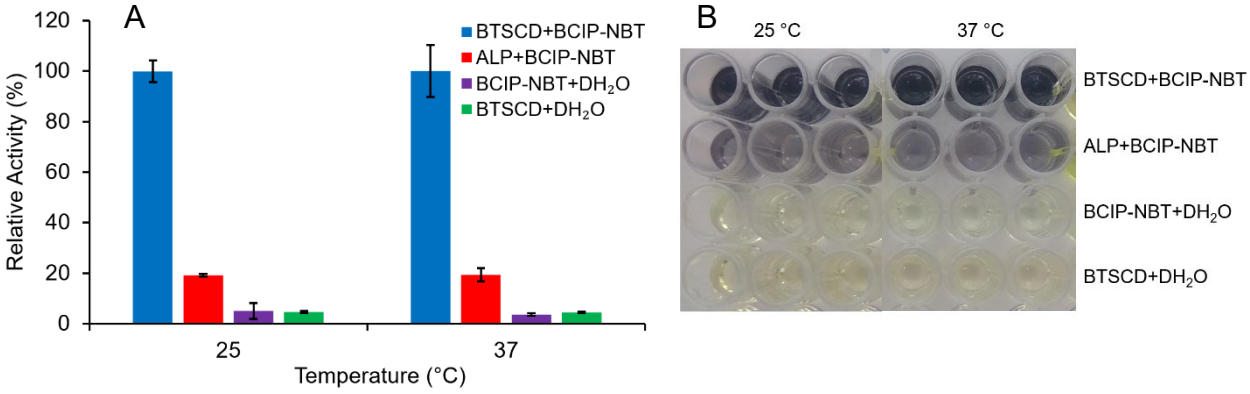

Figure 8. BTSCD temperature assay with BCIP-NBT. (A) Relative activity of mixtures. (B) Wells after completion of reaction.

4.2.3 Kinetics of phosphatase activity

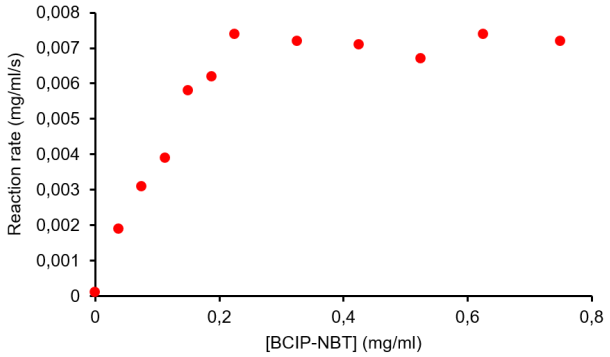

Figure 9. Michaelis-Menten plot of reaction of BTSCD with BCIP-NBT.

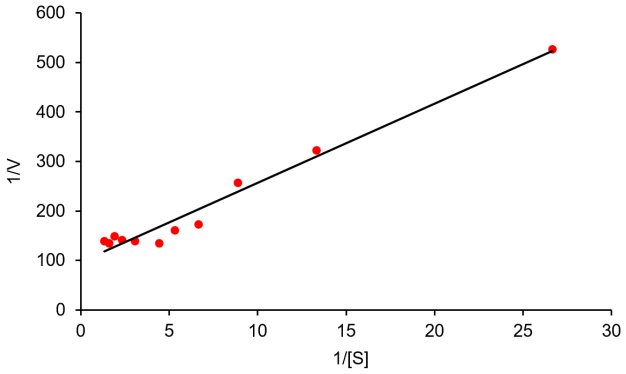

Figure 10. Lineweaver-Burk plot of reaction of BTSCD with BCIP-NBT.

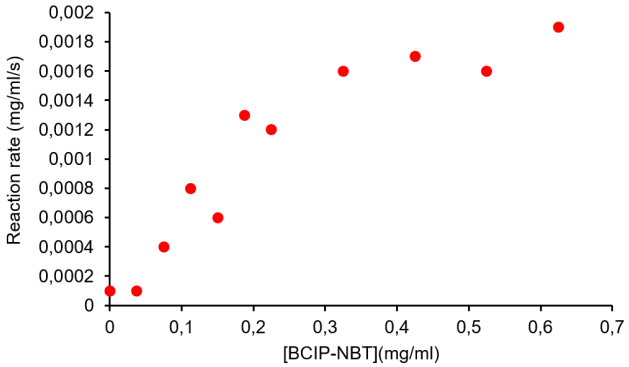

Figure 11. Michaelis-Menten plot of reaction of ALP with BCIP-NBT.

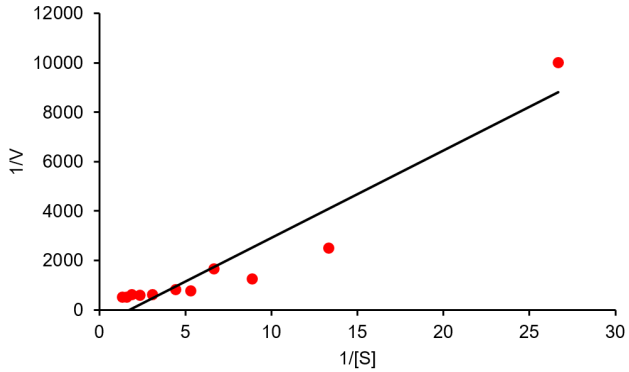

Figure 12. Lineweaver-Burk plot of reaction of ALP with BCIP-NBT.

4.3 BTSCD show moderate phosphatase activity with pNPP and no inhibition by Cu^{2+} ions

4.3.1 pH screening

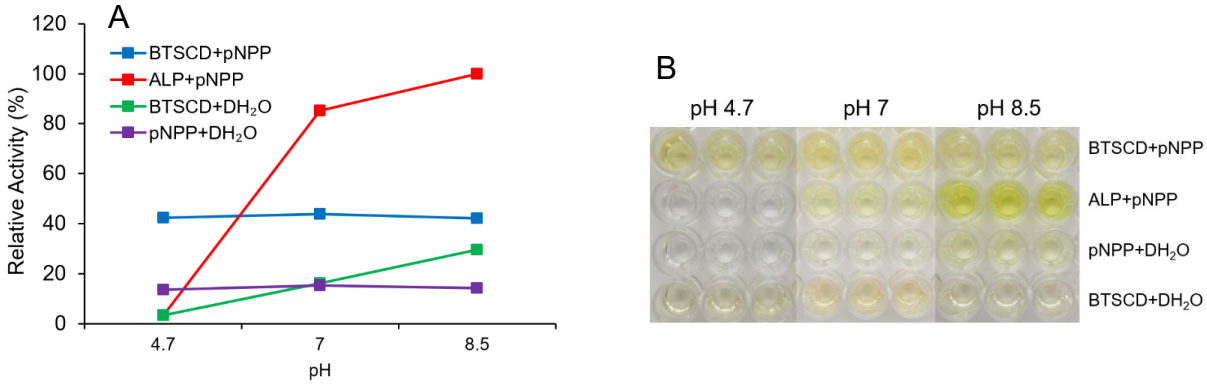

Figure 13. BTSCD pH assay with pNPP. (A) Relative activity of mixtures. (B) Wells after completion of reaction.

4.3.2 Temperature screening

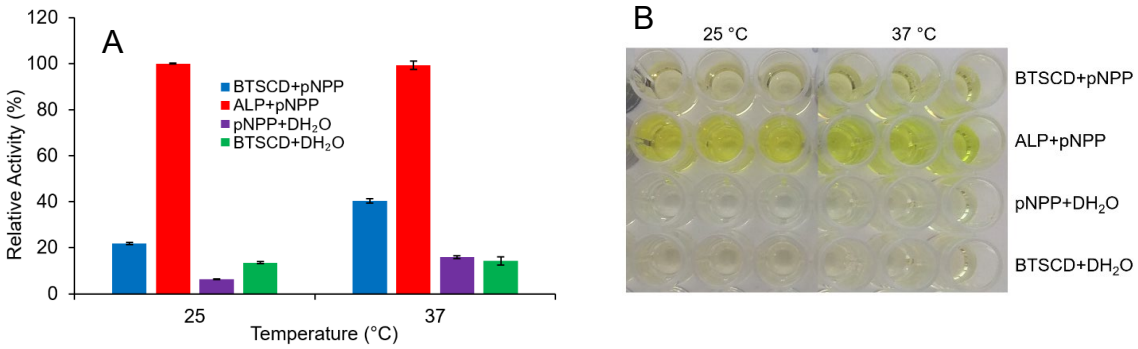

Figure 14. BTSCD temperature assay with pNPP. (A) Relative activity of mixtures. (B) Wells after completion of reaction.

4.3.3 Inhibition screening

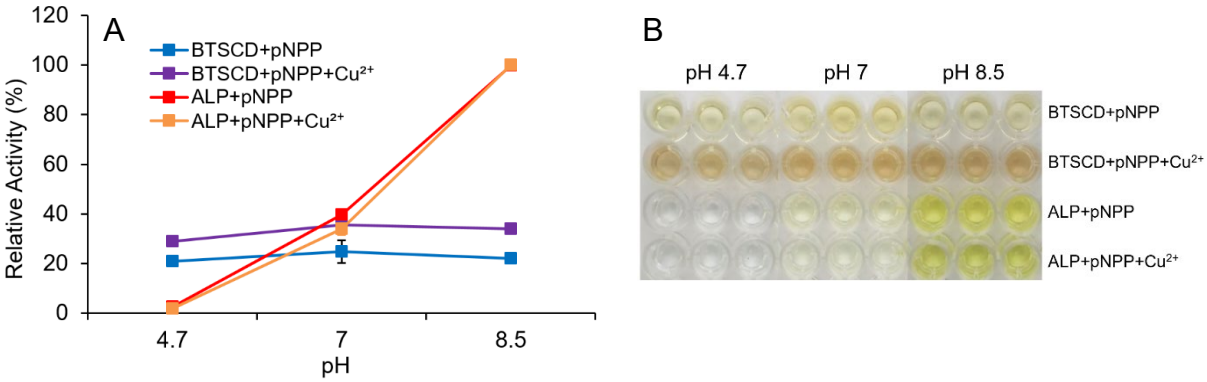

Figure 15. BTSCD Cu^{2+} inhibition assay with pNPP. (A) Relative activity of mixtures. (B) Wells after completion of reaction.

4.4 BTSCD exhibit dose dependent growth inhibition of *E. coli* and *L. lactis*, and ALP might not affect the growth of *E. coli*

4.4.1 *E. coli* screening

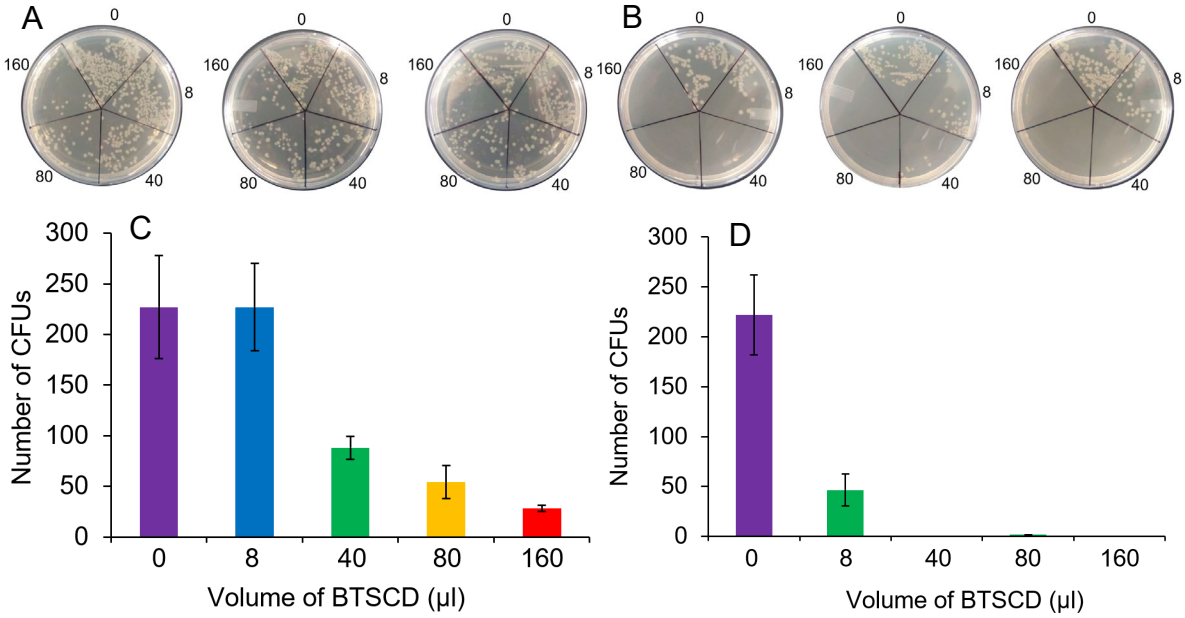

Figure 16. The effect of BTSCD on growth of *E. coli*. (A) Petri dishes with 0.1 mg/ml BTSCD medium. (B) Petri dishes with 0.5 mg/ml BTSCD medium. (C) Number of CFUs grown in 0.1 mg/ml BTSCD. (B) Number of CFUs grown in 0.5 mg/ml BTSCD.

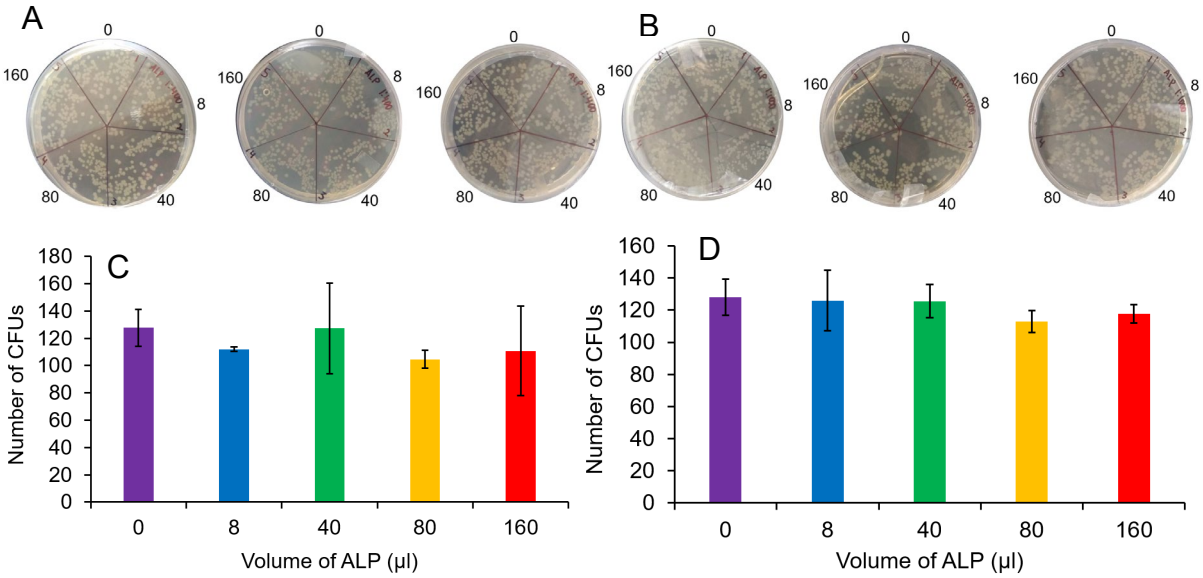

Figure 17. The affect of ALP on growth of *E. coli*. (A) Petri dishes with 1:400 diluted ALP medium. (B) Petri dishes with 1:1000 diluted ALP medium. (C) Number of CFUs grown in 1:400 diluted ALP. (D) Number of CFUs grown in 1:1000 diluted ALP.

4.4.2 *L. lactis* screening

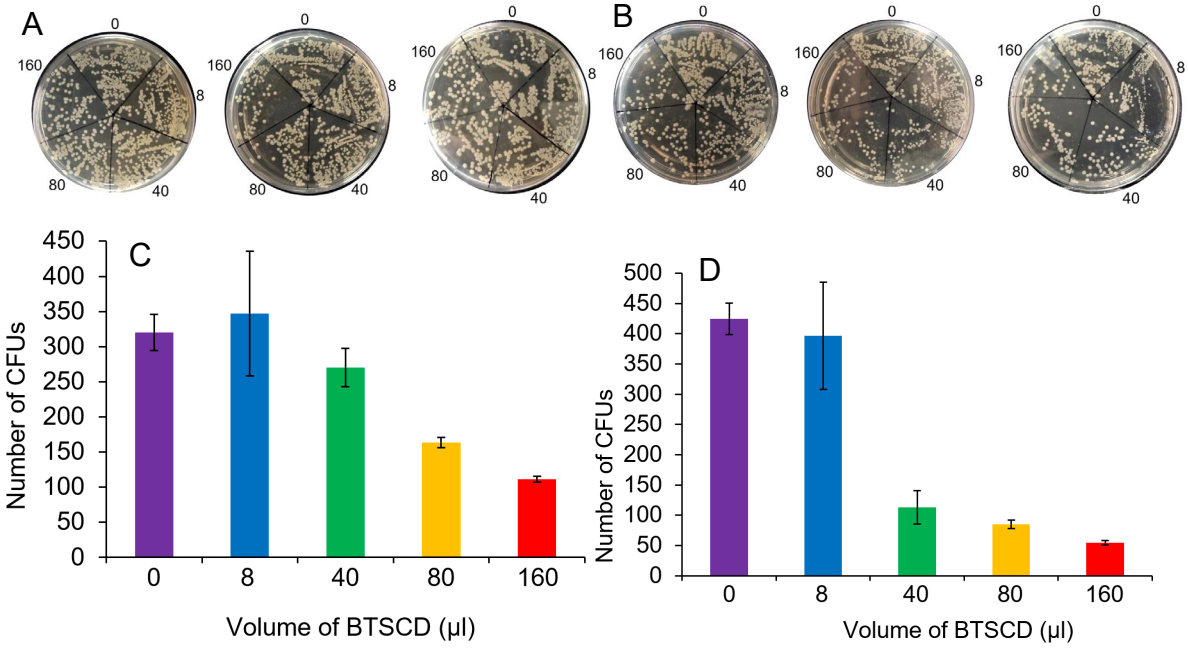

Figure 18. The effect of BTSCD on growth of *L. lactis*. (A) Petri dishes with 0.1 mg/ml BTSCD medium. (B) Petri dishes with 0.5 mg/ml BTSCD medium. (C) Number of CFUs grown in 0.1 mg/ml BTSCD. (B) Number of CFUs grown in 0.5 mg/ml BTSCD.

medium with BTSCD.

5 DISCUSSION

5.1 BTSCD fluoresce at 450 nm, contain C-S bond with amide groups and assemble into ring-shaped particles

5.1.1 Fluorescence spectroscopy

Figure 4 illustrates the fluorescence spectra of three aqueous solutions of BTSCD. All solutions emit fluorescence at 450 nm. The solution with highest concentration of BTSCD, 0.5 mg/ml has the lowest fluorescence intensity out of all of them. The reason for this is that at high concentrations there is self-quenching of CDs. In this process CDs tend to densely pack and severely reduce the fluorescence signal. Lowering the concentration down to 0.2 mg/ml produces so much intensity that the signal is saturated. This is because diluting the solution causes CDs to separate and thus produce higher signal. Thus, high number of surface groups emit strong fluorescence and produce saturated signal. The lowest concentration of BTSCD, 0.05 mg/ml, exhibit signal which is lower than that of solution with 0.2 mg/ml. Diluting the solution more leads to decrease in overall number of segregated CDs and this results in decrease of fluorescence intensity (Yan et al., 2019).

5.1.2 FT-IR

Figure 5 illustrates the FT-IR spectra of doped and non-doped CDs. First, there is peak at 3300 cm^{-1} which indicates the O-H stretching of hydroxyl group in both BT and BTSCD. Second, broad peak at about 2950 cm^{-1} indicates the N-H stretching of amine group in both CDs. Third, strong peak at 1680 cm^{-1} shows C=O stretching of amide group in BTSCD but not in BTCD. Fourth, medium peak at 1590 cm^{-1} shows N-H bending of amine group in both CDs. Five, there are two peaks at 1500 cm^{-1} and 1550 cm^{-1} which indicate the presence of amide backbone in BTCD. Lastly, there are two peaks of BTSCD spectrum which are not present in BTCD spectrum. These peaks are at 980 cm^{-1} and 770 cm^{-1}. Peak at 980 cm^{-1} shows H-S-C bending vibration and peak at 770 cm^{-1} shows C-S stretching. These two peaks indicate the presence of C-S covalent bond in the structure of BTSCD but not in BTCD, therefore, sulfur was successfully added to CDs via hydrothermal treatment. Eventually, BTSCD has hydroxyl, amine and amide groups, as well as, C-S covalent bonds in its structure (https://www.sigmaaldrich.com/technical-documents/articles/biology/ir-spectrum-table.html).

5.1.3 SEM

The figure 6 represents SEM images of BTSCD. Circular particles seen on these pictures are the ring-shaped assemblies of CDs. These assemblies were determined to be 30-40 nm in diameter. Thus, BTSCD tends to form larger particles and perform its function in such state.

5.2 BTSCD exhibit high phosphatase activity with BCIP-NBT and high affinity to it

5.2.1 pH screening

The figure 7A illustrates the line graph of RA of BTSCD in reaction with BCIP-NBT in three pH conditions (4.7, 7, and 8.5). The figure 7B shows the pictures of wells after the completion of reaction. Ideally, the hydrolysis of BCIP forms the 5-bromo-4-chloro-3-indoxyl intermediate which then tends to dimerize into “dehydroindigo” product under alkaline conditions. During dimerization hydrogen ions are released from this product and cause reduction of NBT yielding insoluble NBT formazan which is dark blue to purple color (https://www.sigmaaldrich.com/technical-documents/articles/biofiles/colorimetric-alkaline.html). Two negative controls, BCIP-NBT+DH_2O and BTSCD+DH_2O, showed least RA ranging from 15% to 25% across all three pH conditions. Also calculated p-values show that they were significantly different from test mixture of BTSCD+BCIP-NBT in all pH conditions ($p << 0.05$). This is because there were no reactions, and therefore, no yield in product. Positive control, ALP+BCIP-NBT, also showed low RA in pH 4.7 and pH 7, but

higher activity than negative controls in pH 8.5. This is because ALP, as its name suggests, can only function in alkaline solutions. In pH 8.5 ALP showed about 30% of RA and it can be seen on figure 6B. There is some color change towards dark blue. ALP reacted with BCIP-NBT and was able to remove phosphate group from it, but not as effective as BTSCD. In fact, the relative activities of ALP+BCIP-NBT mixtures in all pH conditions were significantly different from those of BTSCD. The reason for that is low concentration of ALP. BTSCD, on the other hand, showed the highest RA out of all four mixtures, with about 63% at pH 4.7, 100% at pH 7 and 65% at pH 8.5. It can be seen on picture B, where the mixtures turned dark blue and almost black in color. High standard deviation at pH 7 may be due to pipetting error. Acidic and basic conditions almost equally affect the ability of BTSCD to chop phosphate groups. Neutral pH condition was most favorable for BTSCD. Thus, amine groups and sulfur on the surface were able to mimic active center of protein phosphatase and perform the phosphatase reaction. Such dark blue color may suggest that all of BCIP-NBT was chopped into BCIP, NBT and P_i. This may be due to large number of surface groups which were able to remove multiple phosphates at the same time.

5.2.2 Temperature screening

Figure 8A shows the bar chart of RA of BTSCD at 25℃ and 37℃. Figure 8B illustrates the pictures of wells after the completion of reaction. Again, two negative controls, BCIP-NBT+DH_2O and BTSCD+DH_2O, showed least relative activities ranging from about 5% to 8% at both temperatures. Both controls were significantly different from BTSCD+NBT/BCIP mixture at both temperatures. The reason for that is absence of reaction, and therefore no production of chromogenic product. Positive control, ALP+BCIP-NBT, showed a bit higher RA of about 20% at each temperature. On figure 8B it is seen ALP was able to perform phosphatase reaction and yield purple BCI. However, RA of ALP was significantly lower than that of BTSCD. This is due to the low concentration of ALP. BTSCD exhibited the highest RA at both temperatures, 100% at 37℃ and about 98% at 25℃, and yielded enough product to produce dark blue color of mixture. Such high RA values can be from high concentration of BTSCD. High standard deviation may be due to pipetting error. Both temperatures did not affect activity of ALP and BTSCD, which suggest that these compounds are equally active at 25℃ and 37℃. Also, no effect of temperature on BTSCD may be due to high concentration of BTSCD. Thus, BTSCD can perform well at body temperature and its optimum conditions for reaction with BCIP-NBT are pH 7 and 37℃.

5.2.3 Kinetics of phosphatase activity

On figure 9 Michaelis-Menten graph is shown for the reaction of BTSCD with BCIP-NBT. It can be seen that CDs were able to continuously bind molecule of BCIP-NBT, cleave the phosphate, release the products and bind another molecule of BCIP-NBT with gradual saturation of surface groups. It was determined from the Lineweaver-Burk plot on the next figure 10, that the V_{max} for BTSCD was 0.0103 mg/ml/s. Also, K_m was determined and its value was 0.1674. On next figures 11 and 12 there are Michaelis-Menten and Lineweaver-Burk plots for ALP's reaction. Comparing these graphs to those of BTSCD, it can be stated that ALP tends to saturate slower than BTSCD. Also, ALP tends to react slower than BTSCD. In fact, V_{max} for ALP was 0.0016 mg/ml/s and K_m was 0.5715. K_m of ALP is higher than that of BTSCD. It means that ALP has lower affinity to BCIP-NBT than BTSCD. Low speed and affinity of ALP can be explained by larger number of sulfur-containing groups on the surface of BTSCD and lower concentration of ALP stock. Thus, BTSCD may have more than two "active sites" and due to large surface area, may hydrolyze substrate more quickly than ALP. It is known that ALP is usually a multi-substrate enzyme that can bind various phosphate esters. Our CIALP is not an exception. Its active site might be not specific for BCIP and therefore it has low affinity to it. Whereas surface groups of BTSCD might have created extensive "active sites" with electron density and flow suitable for hydrolysis of BCIP and therefore it has higher affinity to BCIP-NBT.

5.3 BTSCD show moderate phosphatase activity with pNPP and no inhibition by Cu^{2+} ions

5.3.1 pH screening

Figure 13A illustrates the line graph of RA of BTSCD with pNPP in three pH buffers (4.7, 7 and 8.5). Figure 13B shows the pictures of wells after the completion of reaction. Proper phosphatase reaction with pNPP should a product of pNP which is bright yellow in color. Two negative controls, pNPP+DH_2O and BTSCD+DH_2O, showed least RA because of the absence of reaction. The control of pNPP+DH_2O showed almost the same RA across all pH conditions, ranging from 14% to 17%. This is because pNPP itself is yellow in color and tends to absorb some of the 405 nm wavelength. The control of BTSCD+DH_2O showed increasing RA starting from approximately 3% in pH 4.7, continuing with 18% in pH 7 and ending with 30% in pH 8.5. Both controls were significantly different from test mixture. BTSCD exhibited almost the same RA across all pH conditions with about 42-45%. As in previous part with BCIP-NBT, pH did not affect the activity of BTSCD. Also, BTSCD was able to do the phosphatase reaction

with pNPP but not as strong as with BCIP-NBT. The reason for this is that pNPP is a substrate made for alkaline solutions. Thus, increasing pH favors the reaction of ALP and results in higher RA of ALP (85% in pH 7 and 100% in pH 8.5). However, BTSCD still hydrolyzed pNPP and was better at it in acidic solutions than ALP (about 3% in pH 4.5). ALP's 100% in pH 8.5 is the ideal standard reaction with pNPP and its attributed to ALP's ability to perform catalysis in alkaline solutions. The lowest RA of ALP in pH 4.7 is from acidic condition which affected the ALP and, thus, reduced its ability to cleave phosphates. All RAs of ALP were significantly different from those of BTSCD.

5.3.2 Temperature screening

Figure 14A shows bar chart of RA of BTSCD in reaction with pNPP at 25℃ and 37℃. Figure 14B illustrates corresponding pictures of the well after completion of reaction. In this part of assay, again, negative controls, pNPP+DH_2O and BTSCD+DH_2O, showed the least relative activities ranging from 6% to 17%. This is due to the absence of reaction. BTSCD mixture showed higher relative activities at both temperatures, 22% at 25℃ and 39% at 37℃. This suggests that there was phosphatase reaction with pNPP which yielded the product of pNP of bright yellow color. The higher RA at 37℃ suggests that higher temperature speeded up the reaction thus, hydrolyzing more pNPP molecules and yielding more chromogenic substrate. Both controls were significantly different from BTSCD at both temperatures. ALP showed the highest RA of 100% at both temperatures. The reason for this is that pNPP is specific substrate made for alkaline solutions. The RAs of ALP were significantly different from RAs of BTSCD at both temperatures. Thus, with pH 8 buffer, pNPP was fully hydrolyzed by ALP and showed the highest RA. The results of reaction are clearly seen on figure 14B.

5.3.3 Inhibition screening

On figure 15A there is line graph of RA of BTSCD and ALP with and without Cu^{2+} inhibitor in three pH conditions (4.7, 7 and 8.5). On figure 15B there are corresponding pictures of wells with completed reactions. It can be seen that BTSCD, with and without Cu^{2+}, exhibited almost the same RA across all pH range. It was ranging from 21% to 24% without inhibitor, and ranging from 30% to 37% in the presence of inhibitor. This result is because Cu^{2+} changed the color of final mixtures and thus affected the absorbance. If there was no change in color, the RA of BTSCD+pNPP+Cu^{2+} mixture would be the same as the RA of BTSCD+pNPP mixture. ALP, on the other hand, was not affected by Cu^{2+} except minor changes in pH 7 buffer. Here ALP with Cu^{2+} was less active than ALP without Cu^{2+}. Thus, the RA of ALP with Cu^{2+} was

about 36% and the RA of ALP without Cu^{2+} was approximately 39%. In other pH buffers, the results were almost same. In pH 4.7 it was around 2% and in pH 8.5 – about 100%. The reason for such low activity is the acidic pH condition which is not suitable for both ALP and pNPP, and, conversely, the reason for 100% RA is the alkaline condition which is fully suitable for both ALP and pNPP. Overall, Cu^{2+} ions did not inhibit neither BTSCD nor ALP. For BTSCD, it may be that there are no sites for ions to attach to. In case of ALP, it is because Cu^{2+} are designed to inhibit protein phosphatases and not alkaline phosphatases.

5.4 BTSCD exhibit dose dependent growth inhibition of *E. coli* and *L. lactis*, and ALP might not affect the growth of *E. coli*

5.4.1 *E. coli* screening

The figures 16A and 16B show the Petri dishes after cultivation of *E. coli* in medium with BTSCD. On the figures 16C and 16D there are bar charts of number of CFUs versus the volume of BTSCD. From the volume and initial concentration, the final concentration of BTSCD was calculated. For the dose of 0.1 mg/ml it was as follows: for 0 µl – 0 mg/ml, for 8 µl – 0.001 mg/ml, for 40 µl – 0.005 mg/ml, for 80 µl – 0.01 mg/ml and for 160 µl – 0.02 mg/ml. For the dose of 0.5 mg/ml it was as follows: for 0 µl – 0 mg/ml, for 8 µl – 0.005 mg/ml, for 40 µl – 0.025 mg/ml, for 80 µl – 0.05 mg/ml and for 160 µl – 0.086 mg/ml. From the chart C it can be seen that there is dose dependent growth inhibition of *E. coli*. Thus, starting from the 0.005 mg/ml (40 µl) there is significant gradual decrease in number of CFUs with about 84 CFUs in 0.005 mg/ml, 66 CFUs in 0.01 mg/ml and 33 CFUs in 0.02 mg/ml. 0.001 mg/ml did not affect the growth of *E. coli* and the number of CFUs was a bit higher than in control. This might be due to spreading of bacteria to the area of control. From the chart D it can be seen that there is complete growth inhibition starting from 0.025 mg/ml. In 0.005 mg/ml there are about 47 CFUs which is significantly lower than in control. Such difference from chart C might be due to spreading of medium from neighboring areas and thus inhibiting the growth. Inhibition of growth can be seen on figures A and B. The antibacterial effect of BTSCD might be due to two reasons. One possible explanation is that BTSCD might have high phosphatase activity and was able to cleave phosphate groups from phospholipids. *E. coli* is the Gram-negative bacteria with thin layer of peptidoglycan and outer membrane before cytoplasmic membrane. The outer membrane of *E. coli* consists of phospholipids and lipoproteins which might be an easy target for BTSCD. Thus, CDs might possibly cleaved the phosphate groups from phospholipids and lipoproteins of outer membrane, possibly broke the linkages between lipoprotein and peptidoglycan leading to collapse of peptidoglycan layer, and, possibly, caused disruption in

the cell wall. To confirm this, bacterial growth assay needs to be done with higher ALP concentration to see if ALP can have the same effect. Another possible explanation is that antibacterial effect may come from electrostatic adhesion of BTSCD to cell wall. It was determined by agarose gel electrophoresis that BTSCD possess positive charge. Therefore, BTSCD might have assembled into larger ring-shaped particles with ultra-positive charge. These cationic particles might possibly have attached to negatively-charged cell wall of *E. coli*, possibly caused cell wall dislocation and might led to cell wall disruption.

The figures 17A and 17B illustrate the Petri dishes after cultivation of *E. coli* in medium with ALP. On figures 17C and 17D there are bar charts of number of CFUs versus the volume of ALP. It can be seen from images and charts that any dose of ALP in both dilutions did not affect the growth of bacteria significantly. This is due to following reasons. First, because of low stock concentration of ALP. Second, the pH of the medium was approximately 6.5 which is slightly acidic. This pH condition is not optimal for ALP to have maximum activity. Third, ALP is a membrane-bound enzyme that is mostly hydrophobic and built in such way to perform its function in cell membrane. Here ALP probably was not bound to any cell membrane and was free in slightly acidic medium. This condition probably affected its function and ALP possibly was not able hydrolyze phosphates as effectively as in location of cell membrane. Fourth, ALP does not have strong affiliation to the cell wall. Therefore, it does not bind phospholipids strongly and does not hydrolyze them. And fifth, ALP is structured in a different way than BTSCD and, therefore, has different mechanism of action than BTSCD. Hided active sites of ALP were not able to reach densely situated phospholipids and perform hydrolysis. BTSCD, on the hand, due its vast number of surface groups and big surface area were possibly able to reach phospholipids and perform hydrolysis.

5.4.2 *L. lactis* screening

The figures 18A and 18B show the Petri dishes after cultivation of *L. lactis* in medium with BTSCD. On the figures 18C and 18D there are bar charts of number of CFUs versus the volume of BTSCD. From the volume and initial concentration, the final concentration of BTSCD was calculated. For the dose of 0.1 mg/ml it was as follows: for 0 µl – 0 mg/ml, for 8 µl – 0.001 mg/ml, for 40 µl – 0.005 mg/ml, for 80 µl – 0.01 mg/ml and for 160 µl – 0.02 mg/ml. For the dose of 0.5 mg/ml it was as follows: for 0 µl – 0 mg/ml, for 8 µl – 0.005 mg/ml, for 40 µl – 0.025 mg/ml, for 80 µl – 0.05 mg/ml and for 160 µl – 0.086 mg/ml. From the chart C it can be seen that there is dose dependent growth inhibition of *L. lactis*. This inhibition is seen in 0.01 mg/ml (162 CFUs) and in 0.02 (117 CFUs). In 0.005 mg/ml there was not significant difference

in number of CFUs but still certain degree of toxicity. In 0.001 mg/ml there was higher number of CFUs than in control. This can be due spreading of some bacteria to the area of control during streaking. Thus, 0.001 mg/ml is non-inhibitory dose of BTSCD. From the chart D it can be seen that there is more toxicity with higher doses. The doses of 0.025 mg/ml, 0.05 mg/ml and 0.086 mg/ml showed significant gradual growth reduction, with the number of CFUs being 113, 86 and 62 respectively. The dose of 0.005 repeats the results from chart C. Corresponding growth inhibition can be seen on images A and B. One possible explanation of this difference in toxicity compared to *E. coli* results is due to structure of cell wall. *L. lactis* is the Gram-positive bacteria with only thick layer of peptidoglycan before cytoplasmic membrane. This layer does not contain any phosphate groups other than lipoteichoic acid which has glycerol phosphate in its structure. Thus, BTSCD may have been attacked those phosphate groups of glycerol and, thereby, partially disrupt the structure of cell wall. This might led to lower levels of leakage and thus, lower inhibition of growth than in *E. coli*. To confirm this bacterial growth assay needs to be done with high ALP concentration. Another possible explanation is, again, due to electrostatic adhesion of BTSCD to cell wall. *L. lactis* has thicker cell wall than in *E. coli* and therefore BTSCD probably caused cell wall dislocation without disruption. Thus, *L. lactis* may be more resistant to the effect of BTSCD.

To determine the exact antibacterial effect of BTSCD following studies need to be done. HR-AFM - to determine exact structure of ring-shaped particles. Zeta potential of BTSCD needs to be determined to confirm the electrostatic adhesion mechanism. SEM needs to be done to see the effect of BTSCD on bacterial cell walls.

In conclusion, it can be stated that sulfur-doped CDs emit fluorescence at 450 nm and have N and S containing groups on surface. Also, these CDs have phosphatase activity and can hydrolyze BCIP-NBT and pNPP. Furthermore, BTSCD can have antibacterial effect on *E. coli* and *L. lactis*. Action of BTSCD on bacteria is unclear and requires more studies to understand the exact mechanism of antibacterial effect.

6 REFERENCES

1. Abcam. (2020). *ab83369 Alkaline Phosphatase Assay Kit (Colorimetric)*. Retrieved from https://www.abcam.com/ps/products/83/ab83369/documents/alkaline-phosphatase-assay-kit-protocol-book-v12-ab83369%20(website).pdf
2. Anwar S, Ding H, Xu M, Hu X, Li Z,Wang J, Liu L, Jiang L, Wang D, Dong C, Yan M, Wang Q & Bi H (2019) Recent advances in synthesis, optical properties, and biomedical applications of carbon dots. *ACS Appl. Bio Mater* **2:** 2317–2338
3. Baker SN & Baker GA (2010) Luminescent Carbon Nanodots: Emergent Nanolights. *Angewandte Chemie International Edition* **49:** 6726–6744
4. Buchet R, Millán JL & Magne D (2013) Multisystemic Functions of Alkaline Phosphatases. *Methods in Molecular Biology Phosphatase Modulators* **1053:** 27-51
5. Cao L, Wang X, Meziani MJ, Lu F, Wang H, Luo PG, Lin Y, Harruff BA, Veca LM, Murray D, Xie S-Y & Sun Y-P (2007) Carbon Dots for Multiphoton Bioimaging. *Journal of the American Chemical Society* **129:** 11318–11319
6. Cayuela A, Soriano ML, Carrilo-Carrión C & Valcárcel M (2016) Semiconductor and carbon-based fluorescent nanodots: the need for consistency. *Chemical Communications* **52:** 1311-1326.
7. Chatzimitakos TG, Kasouni AI, Troganis AN & Stalikas CD (2020) Exploring the antibacterial potential and unraveling the mechanism of action of non-doped and heteroatom-doped carbon nanodots. *Journal of Nanoparticle Research* **22**
8. Chen Y-C, Nien C-Y, Albert K, Wen C-C, Hsieh Y-Z and Hsu H-Y (2016). Pseudo-multicolor carbon dots emission and the dilution-induced reversible fluorescence shift. *RSC Advances* **6:** 44024–44028.
9. Das T, Saikia BK, Dekaboruah H, Bordoloi M, Neog D, Bora JJ, Lahkar J, Narzary B, Roy S & Ramaiah D (2019) Blue-fluorescent and biocompatible carbon dots derived from abundant low-quality coals. *Journal of Photochemistry and Photobiology B: Biology* **195:** 1–11
10. Dean RL (2002) Kinetic studies with alkaline phosphatase in the presence and absence of inhibitors and divalent cations. *Biochemistry and Molecular Biology Education* **30:** 401-407
11. Dou Q, Fang X, Jiang S, Chee PL, Lee T-C & Loh XJ (2015) Multi-functional fluorescent carbon dots with antibacterial and gene delivery properties. *RSC Advances* **5**: 46817-4
12. Garg B & Bisht T (2016) Carbon Nanodots as Peroxidase Nanozymes for Biosensing. *Molecules* **21:** 1653
13. Haarhaus M, Brandenburg V, Kalantar-Zadeh K, Stenvinkel P & Magnusson P (2017) Alkaline phosphatase: A novel treatment target for cardiovascular disease in CKD. *Nature Reviews Nephrology* **13:** 429-442
14. Havrdova M, Hola K, Skopalik J, Tomankova K, Petr M, Cepe K, Polakova K, Tucek J, Bourlinos AB & Zboril R (2016) Toxicity of carbon dots – Effect of surface functionalization on the cell viability, reactive oxygen species generation and cell cycle. *Carbon* **99:** 238-248

15. He L, Wang T, An J, Li X, Zhang L, Li L, Li G, Wu X, Su Z & Wang C (2014) Carbon nanodots@zeolitic imidazolate framework-8 nanoparticles for simultaneous pH-responsive drug delivery and fluorescence imaging. *CrystEngComm* **16:** 3259
16. Hsu P-C, Shih Z-Y, Lee C-H & Chang H-T (2012) Synthesis and analytical applications of photoluminescent carbon nanodots. *Green Chemistry* **14:** 917
17. https://www.ebi.ac.uk/pdbe/entry/pdb/1alk%20%20 Accessed on 30-10-20
18. https://www.sigmaaldrich.com/technical-documents/articles/biofiles/colorimetric-alkaline.html Accessed on 06-11-20
19. https://www.sigmaaldrich.com/technical-documents/articles/biology/ir-spectrum-table.html Accessed on 05-11-20
20. Jian H-J, Wu R-S, Lin T-Y, Li Y-J, Lin H-J, Harroun SG, Lai J-Y & Huang C-C (2017) Super-Cationic Carbon Quantum Dots Synthesized from Spermidine as an Eye Drop Formulation for Topical Treatment of Bacterial Keratitis. *ACS Nano* **11:** 6703-6716
21. Kim EE & Wyckoff HW (1991) Reaction mechanism of alkaline phosphatase based on crystal structures. *Journal of Molecular Biology* **218:** 449-464
22. Lakowicz JR (2010) Principles of fluorescence spectroscopy New York, New York: Springer Science+Business Media
23. Li C-L, Ou C-M, Huang C-C, Wu W-C, Chen Y-P, Lin T-E, Ho L-C, Wang C-W, Shih C-C, Zhou H-C, Lee Y-C, Tzeng W-F, Chiou T-J, Chu S-T, Cang J & Chang H-T (2014) Carbon dots prepared from ginger exhibiting efficient inhibition of human hepatocellular carcinoma cells. *Journal of Materials Chemistry B* **2:** 4564
24. Li H, Kang Z, Liu Y & Lee S-T (2012) Carbon nanodots: synthesis, properties and applications. *Journal of Materials Chemistry* **22:** 24230
25. Li H, Huang J, Song Y, Zhang M, Wang H, Lu F, Huang H, Liu Y, Dai X, Gu Z, Yang Z, Zhou R & Kang Z (2018) Degradable Carbon Dots with Broad-Spectrum Antibacterial Activity. *ACS Applied Materials & Interfaces* **10:** 26936-26946
26. Lim SY, Shen W & Gao Z (2015) Carbon quantum dots and their applications. *Chem. Soc. Rev.* **44:** 362–381
27. Liu C, Zhang P, Zhai X, Tian F, Li W, Yang J, Liu Y, Wang H, Wang W & Liu W (2012) Nano-carrier for gene delivery and bioimaging based on carbon dots with PEI-passivation enhanced fluorescence. *Biomaterials* **33:** 3604–3613
28. Liu J, Li D, Zhang K, Yang M, Sun H & Yang B (2018) One-step hydrothermal synthesis of nitrogen-doped conjugated carbonized polymer dots with 31% efficient red emission for in vivo imaging. *Small* **14:** 1703919
29. Liu R, Wu D, Liu S, Koynov K, Knoll W & Li Q (2009) An Aqueous Route to Multicolor Photoluminescent Carbon Dots Using Silica Spheres as Carriers. *Angewandte Chemie* **121:** 4668–4671
30. Liu S, Yu B & Zhang T (2014) Nitrogen-doped carbon nanodots as a reducing agent to synthesize Ag nanoparticles for non-enzymatic hydrogen peroxide detection. *RSC Adv.* **4:** 544–548

31. Lv Y, Ma M, Huang Y & Xia Y (2018) Carbon Dot Nanozymes: How to Be Close to Natural Enzymes. *Chemistry – A European Journal* **25:** 954-960
32. Merck KGaA. (2020). *Culture of E. coli.* Retrieved from https://www.sigmaaldrich.com/technical-documents/protocols/biology/microbial-growth.html
33. Miao P, Han K, Tang Y, Wang B, Lin T & Cheng W (2015) Recent advances in carbon nanodots: synthesis, properties and biomedical applications. *Nanoscale* **7:** 1586–1595
34. Na N, Liu T, Xu S, Zhang Y, He D, Huang L & Ouyang J (2013) Application of fluorescent carbon nanodots in fluorescence imaging of human serum proteins. *J. Mater. Chem. B* **1:** 787–792
35. Nelson DL (2013) Enzymes. In *Lehninger principles of biochemistry* pp 189–242. New York, New York: W H Freeman
36. Nesmeyanova MA, Motlokh OB, Kolot MN & Kulaev IS (1981) Multiple forms of alkaline phosphatase from Escherichia coli cells with repressed and derepressed biosynthesis of the enzyme. *Journal of Bacteriology* **146:** 453-459
37. Qiao Z-A, Wang Y, Gao Y, Li H, Dai T, Liu Y & Huo Q (2010) Commercially activated carbon as the source for producing multicolor photoluminescent carbon dots by chemical oxidation. *Chemical Communications* **46:** 8812
38. Qin X, Lu W, Asiri AM, Al-Youbi AO & Sun X (2013) Microwave-assisted rapid green synthesis of photoluminescent carbon nanodots from flour and their applications for sensitive and selective detection of mercury(II) ions. *Sensors and Actuators B: Chemical* **184:** 156–162
39. Sawant VJ & Bamane SR (2016) Antioxidant, Catalytic Reducing and Anticancer Properties from Hydrothermally Green Synthesized Ginger Derived Carbon Nanodots. *Asian Journal of Organic and Medicinal Chemistry* **1:** 112-117
40. Sharma U, Pal D & Prasad R (2013). Alkaline Phosphatase: An Overview. *Indian Journal of Clinical Biochemistry* **29:** 269-278
41. Shen J, Zhu Y, Yang X, Zong J, Zhang J & Li C (2012) One-pot hydrothermal synthesis of graphene quantum dots surface-passivated by polyethylene glycol and their photoelectric conversion under near-infrared light. *New J. Chem.* **36:** 97–101
42. Shi W, Wang Q, Long Y, Cheng Z, Chen S, Zheng H & Huang Y (2011) Carbon nanodots as peroxidase mimetics and their applications to glucose detection. *Chemical Communications* **47:** 6695
43. Štefková K, Procházková J & Pacherník J (2015) Alkaline Phosphatase in Stem Cells. *Stem Cells International* **2015:** 1-11
44. Thermo Fisher Scientific. (2011). *1-Step™ NBT/BCIP.* Retrieved from https://assets.thermofisher.com/TFS-Assets/LSG/manuals/MAN0011289_1Step_NBT_BCIP_UG.pdf
45. Thermo Fisher Scientific. (2012). *1-Step PNPP.* Retrieved from https://assets.thermofisher.com/TFSAssets/LSG/manuals/MAN0011354_1Step_PNPP_UG.pdf
46. Travlou NA, Giannakoudakis DA, Algarra M, Labella AM, Rodríguez-Castellón E & Bandosz TJ (2018) S- and N-doped carbon quantum dots: Surface chemistry dependent antibacterial activity. *Carbon* **135:** 104-111
47. Wang J & Qiu J (2016) A review of carbon dots in biological applications. *Journal of Materials Science* **51:** 4728–4738

48. Wang X, Feng Y, Dong P & Huang J (2019) A Mini Review on Carbon Quantum Dots: Preparation, Properties, and Electrocatalytic Application. *Frontiers in Chemistry* **7:** 671
49. Xu B, Zhao C, Wei W, Ren J, Miyoshi D, Sugimoto N & Qu X (2012) Aptamer carbon nanodot sandwich used for fluorescent detection of protein. *The Analyst* **137:** 5483
50. Xu J, Lai T, Feng Z, Weng X & Huang C (2014) Formation of fluorescent carbon nanodots from kitchen wastes and their application for detection of Fe3+. *Luminescence,* **30:** 420-424
51. Xu X, Ray R, Gu Y, Ploehn HJ, Gearheart L, Raker K & Scrivens WA (2004) Electrophoretic Analysis and Purification of Fluorescent Single-Walled Carbon Nanotube Fragments. *Journal of the American Chemical Society* **126:** 12736-12737
52. Yan F, Jiang Y, Sun X, Wei J, Chen L & Zhang Y (2019) Multicolor carbon dots with concentration-tunable fluorescence and solvent-affected aggregation states for white light-emitting diodes. *Nano Research* **13:** 52–60
53. Zhu S, Meng Q, Wang L, Zhang J, Song Y, Jin H, Zhang K, Sun H, Wang H & Yang B (2013) Highly Photoluminescent Carbon Dots for Multicolor Patterning, Sensors, and Bioimaging. *Angewandte Chemie International Edition* **52:** 3953–3957

7 APPENDICES